


**Pseudospin-1 wave scattering that defies chaos  $Q$ -spoiling and Klein tunneling**Hong-Ya Xu<sup>1</sup> and Ying-Cheng Lai<sup>1,2,\*</sup><sup>1</sup>*School of Electrical, Computer and Energy Engineering, Arizona State University, Tempe, Arizona 85287, USA*<sup>2</sup>*Department of Physics, Arizona State University, Tempe, Arizona 85287, USA* (Received 14 August 2018; revised manuscript received 1 May 2019; published 4 June 2019)

$Q$ -spoiling is a known phenomenon in wave chaos, where an open chaotic cavity deformed from an integrable one exhibits a significantly reduced  $Q$ -value. In relativistic quantum mechanics, another mechanism that makes trapping of waves difficult is Klein tunneling. For chaotic scattering of a pseudospin-1 wave from a deformed scalar potential domain, both “leaking” mechanisms are thus present. Surprisingly, we find an energy range in which a pseudospin-1 chaotic cavity is capable of defying both  $Q$ -spoiling and super-Klein tunneling. The physical origin of this remarkable phenomenon is a peculiar type of unexpectedly robust edge modes that absolutely have no counterpart in nonrelativistic quantum or even in pseudospin-1/2 systems. The phenomenon can be tested experimentally in emerging electronic or photonic metamaterials with pseudospin-1 Dirac cones.

DOI: [10.1103/PhysRevB.99.235403](https://doi.org/10.1103/PhysRevB.99.235403)**I. INTRODUCTION**

A well-established notion in quantum chaos is that classical dynamics defined by the geodesic ray path are relevant in the short wavelength limit when the effective Planck constant approaches zero. Because of this relevance, characteristic and universal fingerprints of classical chaos can emerge in the corresponding wave system [1,2]. Take quantum/wave scattering [3] as an example. For integrable classical dynamics, there can be sharp quantum resonances due to the stable orbits in the scattering region with a divergent lifetime, leading to an algebraic decay of the particles. If the classical dynamics are fully chaotic with no stable periodic orbits, the particle decay is exponential with a finite average lifetime, broadening the quantum resonances. Semiclassical arguments based on the quantum-classical correspondence [4] stipulate that the statistical fluctuation patterns with energy of the quantum scattering matrix elements are characteristically distinct for classical integrable and chaotic dynamics [5–7]. A ray-wave correspondence thus exists, which is believed to be a general and universal principle in physics.

The ray-wave correspondence results in remarkable phenomena such as  $Q$ -spoiling in optics. For example, deformed dielectric microcavities allowing exponentially slow evanescent leakage and refractive escape on the entire boundary [8] can lead to ray chaos, which in the wave picture can drastically reduce the lifetime of high- $Q$  resonant modes via the mechanism of chaos-assisted tunneling. Associated with  $Q$ -spoiling is a highly anisotropic output, which can be expected from the corresponding ray dynamics model [9–11]. A related phenomenon occurs in electronic transport through a ballistic quantum dot [12–17], where classically integrable dynamics often leads to sharp conductance fluctuations with energy or the magnetic field strength. Fully developed chaos, because

of its ability to broaden the isolated narrow resonances, can smooth out the conductance fluctuations. This means that classical chaos can be used to modulate conductance fluctuations [18,19].

In relativistic quantum systems, another mechanism that makes wave trapping or confinement difficult is Klein tunneling, where substantial tunneling can occur even when the potential barrier is wide and the particle energy is below the potential height [20–23]. When both chaos and Klein tunneling are present, intuitively, confinement of the particle for a relatively long time would seem impossible.

In this paper, we present a class of relativistic quantum scattering systems that defy chaos  $Q$ -spoiling and Klein tunneling, *a phenomenon that absolutely breaks the ray-wave correspondence*. It occurs in Dirac material systems hosting pseudospin-1 quasiparticles with a conical intersection of triple degeneracy in the underlying energy band [24–51], whose physics is described by the generalized Dirac-Weyl equation for massless spin-1 particles [25,26,44]. Pseudospin-1 quasiparticles are different from Dirac, Weyl, and Majorana fermions, and are of particular interest to the broad research community with diverse experimental realization schemes such as artificial photonic lattices [30,34,38,39,42,52,53], optical [40], and electronic Lieb lattices [49,50], as well as superconducting qutrits [51]. A striking relativistic quantum hallmark of pseudospin-1 particles is super-Klein tunneling through a scalar potential barrier [26,28,41,54], where omnidirectional and perfect transmission of probability one occurs when the incident energy is about one half of the potential height. Generally, Klein tunneling defines optical-like, negatively refracted ray paths through the barrier interface via angularly resolved transmittance in the short wavelength limit [55–57]. When both super-Klein tunneling and chaos are present, one may intuitively expect severe leakage to predominantly occur so trapping would be impossible. However, quite counterintuitively, we uncover an energy range in which robust wave confinement occurs in spite of chaos

\*Ying-Cheng.Lai@asu.edu

and super-Klein tunneling. Especially, we find that the three-component spinor wave concentrates in a particular region of the boundary through strongly squeezed local current vortices generated there, whose pattern in physical space can be manipulated in a reconfigurable manner, e.g., by deforming the boundary shape or setting the direction of the excitation wave. While these modes are distributed unevenly in physical space because of the irregular deformations, even fully developed chaos and super-Klein tunneling are not able to reduce their trapping lifetime. That is, these modes break the quantum-classical correspondence totally and completely, contradicting the intuitive expectation that electrostatically confining relativistic type of carriers/particles to a finite chaotic domain is impossible due to the simultaneous presence of two leaking ( $Q$ -spoiling) mechanisms: chaos assisted tunneling and Klein tunneling. This phenomenon has no counterpart in nonrelativistic quantum or even in pseudospin-1/2 systems. The resulting narrow resonances are also characteristically different from those due to scarring modes concentrating on periodic orbits in conventional wave chaotic scattering, in quantum dots [58–64], or in open optical microcavities [9–11], for which there is still a reasonable ray-wave correspondence. A key technical breakthrough that makes the discovery possible is our development of an extremely efficient and accurate method to solve relativistic quantum chaotic scattering of massless spin-1 particles from an electrostatic potential barrier of finite range and arbitrary shape (Appendix A).

## II. PSEUDOSPIN-1 DIRAC-WEYL SYSTEMS

In recent years, a large number of lattice systems have been discovered, which host exotic low-energy, relativistic quantum quasiparticles that have no apparent counterparts with conventional particles (e.g., Dirac, Weyl, and Majorana particles) in high-energy physics [30,35,40,42,44,49,50]. Typically, such lattice systems do not obey the stringent constraints imposed by the Poincaré symmetry but are governed by only certain subgroups of it. Our work focuses on one type of such quasiparticles: pseudospin-1 particles.

Particularly, we study the scattering of pseudospin-1 particles in a planar potential field  $\mathcal{V}(\mathbf{r})$  of finite range whose shape can be chosen to generate classically integrable or chaotic dynamics. For simplicity, we consider a piecewise constant potential, which corresponds to a junction or a dot/cavity device in an experimentally accessible lattice system, a setting that has been widely used in studying the scattering of spin-1/2 Dirac-Weyl particles [65–69] and in graphene-based experiments [70,71]. For scattering of pseudospin-1 waves, super-Klein tunneling can occur, which is characteristically different from conventional Klein tunneling that occurs only at normal incidence in scattering of massless pseudospin-1/2 Dirac fermions [21]. Intuitively, it would then be significantly more difficult to confine pseudospin-1 particles electrostatically than to confine massless pseudospin-1/2 particles. Even for a classically integrable cavity, quasi-bound states could be much less robust against perturbations for pseudospin-1 particles than for pseudospin-1/2 fermions. When the perturbations are strong enough to induce fully developed classical chaos so the two  $Q$ -spoiling mechanisms,

i.e., chaos-assisted tunneling and Klein tunneling, are simultaneously present, any kind of quasibound states would be eliminated for pseudospin-1 particles. Is this intuitive picture true?

The starting point of our study is the effective low-energy Hamiltonian describing the motion of a massless pseudospin-1 particle in the plane  $\mathbf{r} = (x, y)$  under the action of a scalar potential  $\mathcal{V}(\mathbf{r})$ . In the position representation, the Hamiltonian reads

$$\hat{H} = v_F \hat{\mathbf{S}} \cdot \hat{\mathbf{p}} + S_0 \mathcal{V}(\mathbf{r}), \quad (1)$$

where  $v_F$  is the magnitude of the Fermi velocity,  $\hat{\mathbf{S}} = (S_x, S_y)$  are spin-1 matrices,  $\hat{\mathbf{p}}$  is the momentum operator, and  $S_0$  is the three-by-three identity matrix. The particle dynamics with energy  $E$  are governed by the generalized Dirac-Weyl equation for energy eigenstates  $\Psi(\mathbf{r}) = [\psi_1(\mathbf{r}), \psi_2(\mathbf{r}), \psi_3(\mathbf{r})]^T$ :

$$\hat{H} \Psi(\mathbf{r}) = E \Psi(\mathbf{r}). \quad (2)$$

For a spatially homogeneous/constant potential, e.g.,  $\mathcal{V}(\mathbf{r}) = V_0$ , the eigenenergies are  $E = V_0$  and

$$E = V_0 + s \hbar v_F |\mathbf{k}|,$$

with  $s = \pm$  being the dispersive band index, while the corresponding plane-wave solutions can be written as

$$\Psi_{k,0}(\mathbf{r}) = 1/\sqrt{2}[-e^{-i\beta}, 0, e^{i\beta}]^T e^{i\mathbf{k}\cdot\mathbf{r}}$$

and

$$\Psi_{k,s}(\mathbf{r}) = \frac{1}{2} \begin{pmatrix} e^{-i\beta} \\ \sqrt{2}s \\ e^{i\beta} \end{pmatrix} e^{i\mathbf{k}\cdot\mathbf{r}}, \quad (3)$$

where the wave vector  $\mathbf{k} = (k_x, k_y)$  has length  $k = |\mathbf{k}|$  and makes an angle  $\beta = \arctan(k_y/k_x)$  with the  $x$  axis. The current operator is defined from Eq. (1) as

$$\hat{\mathbf{u}} = \nabla_p \hat{H} = v_F \hat{\mathbf{S}}. \quad (4)$$

The local current associated with a given state  $\Psi(\mathbf{r})$  can be calculated from the local expectation value of  $\hat{\mathbf{u}}$  as

$$\begin{aligned} \mathbf{u}(\mathbf{r}) &= v_F (\psi_1^*, \psi_2^*, \psi_3^*) \hat{\mathbf{S}} \begin{pmatrix} \psi_1 \\ \psi_2 \\ \psi_3 \end{pmatrix} \\ &= \sqrt{2} v_F (\Re[\psi_2^*(\psi_1 + \psi_3)], -\Im[\psi_2^*(\psi_1 - \psi_3)]). \end{aligned} \quad (5)$$

Using the plane wave Eq. (3), we obtain  $\mathbf{u} = s v_F \mathbf{k}/k$ . The effects of the applied scalar potential are to shift the Dirac point ( $k = 0$ ) in the energy domain, to tune the particles' kinetic energy  $\epsilon = (E - V_0)/\hbar v_F$ , and to alter their attributes from hole to electron type, and vice versa.

The focus of our paper is on the interplay between relativistic quantum, three-component pseudospinor wave dynamics, and classical chaos. This is different from the commonly studied interplay between pseudospin-1/2 Dirac fermion system and chaos in the field of relativistic quantum chaos [72,73], and also distinct from the existing studies of the three-component SU(3)-model-based quantum nonlinear dynamics

and chaos [74] for systems such as spinor Bose gases in ultracold atomic physics to which relativistic quantum effects are irrelevant.

Our prototypical setting is a two-dimensional potential step (scatterer) of the stadium shape that permits fully developed chaos in the classical limit. Unlike the case of a circular potential barrier where analytic solutions can be obtained [75], analytic treatment of quantum scattering of pseudospin-1 wave from a stadium (chaotic) domain is not possible. Because the classical scattering system is nonintegrable, it cannot simply be reduced to a one-dimensional problem. To our knowledge, prior to our work, not even an effective numerical method existed for the task. We thus seek to develop a feasible and efficient computational method. Mathematically, the problem is to solve the generalized Dirac-Weyl spinor wave equation with given scalar potential steps of an irregular closed shape in the open space, taking into account the physically open boundary conditions. It is effectively a problem of relativistic quantum chaotic scattering of two-dimensional massless pseudospin-1 particles from short-range obstacles in the presence of relativistic-tunneling-based resonant interaction. Because of classical chaos, a Dirac-type of matrix wave equation is nonseparable. While the real-space Green's-function-based boundary element method [76] or more general methods based on the Lippmann-Schwinger equation [6] can in principle be adopted to solving quantum chaotic scattering of spinless or spin-1/2 particles, such methods did not exist for pseudospin-1 particles. In fact, it is extremely difficult to obtain the real-space Green's function for pseudospin-1 waves in a closed form expression due to the emergence of the singularity in the density of state caused by the flat band of the underlying lattice system [77]. To overcome this difficulty, we exploit the close analogy between the massless pseudospin-1 particle and light photon in that they both possess a linear dispersion relation. Specifically, in optics, there exists a multiple multipoles method (method of "fictitious" sources) for treating scattering of electromagnetic waves from a cavity of arbitrary shape [78–82]. We have adopted this method to pseudospin-1 wave scattering systems with an arbitrary piecewise homogeneous potential, where the multipoles or "fictitious" sources are defined in terms of the analytic three-component spinor cylindrical wave basis of the eigensolutions to the generalized Dirac-Weyl equation in each subregion separated by the potential boundaries. The multiple multipole method is thus of the semianalytic type, which is powerful for near-field calculations and is in principle suitable for potential domains of an arbitrary shape. The details of this method are described in Appendix A.

To establish the generality of our finding, we also study pseudospin-1 wave scattering from a class of chaotic cavities with an eccentric annular shape. For such cavity systems, quantum scattering of pseudospin-1/2 particles was recently studied, where the phenomenon of relativistic quantum chimera was uncovered [83]. To solve pseudospin-1 wave scattering from the eccentric annular chaotic cavity, we develop a scattering matrix approach based on wave-function matching, which is extremely efficient for the particular geometric domain. The method is also of the semianalytic type.

### III. QUANTUM CHAOTIC SCATTERING OF PSEUDOSPIN-1 WAVES IN A STADIUM POTENTIAL

#### A. Emergence of edge resonant modes

Contrary to intuition, here we demonstrate the emergence of an *unexpectedly robust class of sharp resonances* associated with massless pseudospin-1 particle scattering, which generate chaos-immune, high- $Q$  confinement of small modal volume at the boundary in the semiclassical regime where the wavelength is short compared with the cavity/dot size. This is surprising as the confining modes occur in the super-Klein tunneling regime with fully developed chaotic ray dynamics, in which the system is expected to be a perfectly transparent lens. According to conventional wisdom, there would be no room for any trapping nodes in the semiclassical sense.

Specifically, we consider the prototypical setting of plane wave incident on the potential barrier region of a stadium shape parameterized by the aspect ratio  $a/R$  [Fig. 1(e)], which generates chaos in the classical limit, and analyze spinor wave scattering and its correspondence with the underlying ray dynamics. This setting is different from that of scattering transport through a quantum dot structure. We first examine the scattering wave functions of an incident plane spinor wave of short wavelength both inside and outside of the scatterer. Representative results are shown in Fig. 1. Due to super-Klein tunneling [Fig. 1(a)] and the defocusing mechanism of classical chaos, semiclassically the scatterer acts as a superlens with the stadium shape, generating a folded (rainbow) caustic pattern inside, which corresponds to the envelope of the negatively refracted ray paths of parallel incident rays, as shown in the upper panel of Fig. 1(b). The corresponding result from the exact wave calculation is shown in the lower panel of Fig. 1(b), which exhibits significant deviations from the classical ray result due to the emergence of peculiar localized states at the straight side boundary. The deviations can be quantified, as demonstrated in Fig. 1(c), where the  $y$ -axis distribution of the integral amplitude intensity over the horizontal range of the shaded domain in Fig. 1(b) is obtained quantum mechanically through  $I_q(y) = \int_{-a}^a \Psi^\dagger(\mathbf{r})\Psi(\mathbf{r})dx$  and semiclassically by  $I_{sc}(y) = \sum_{n \in M_y} \mathcal{P}_n$ . In particular, we discretize the  $y$  axis in small steps of  $h$  and enumerate all segments between successive collisions inside the scatterer, where  $\mathcal{P}_n$  ( $n = 1, 2, \dots$ ) is the survival intensity of the  $n$ th ray segment and  $M_y$  is the number set of rays passing through an element  $\{(x, y') | x \in [-a, a], y' \in [y - h/2, y + h/2]\}$ . For comparison, we include the corresponding results for pseudospin-1/2 Dirac fermion scattering from the same system, as shown in Figs. 1(d)–1(f). In stark contrast to quantum chaotic scattering of pseudospin-1 particles, the scattering of pseudospin-1/2 fermions enjoys a well defined ray-wave correspondence.

We next study the interplay between relativistic quantum wave dynamics and the underlying classical transient chaos from the perspective of scattering resonance, as shown in Fig. 2 through the local density of states (LDOS)  $\propto \Psi^\dagger(\mathbf{r}^*)\Psi(\mathbf{r}^*)$  in the Klein tunneling regime, where  $\mathbf{r}^*$  is a specific position inside the scatterer. For the integrable barrier, there are sharp resonances leading to strong confinement, as shown in Figs. 2(a) and 2(b) for massless pseudospin-1/2 wave (solid orange curve) and pseudospin-1 wave (solid gray

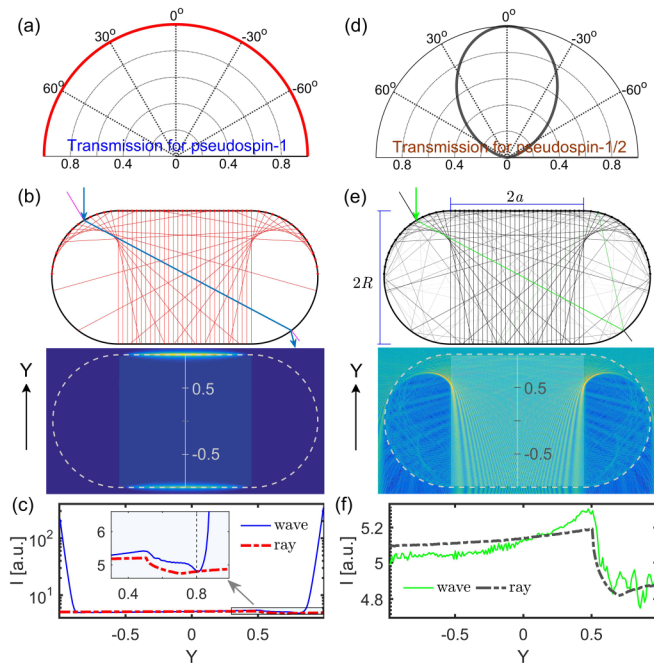


FIG. 1. Caustics anomaly due to the emergent localized modes at the straight side boundary in the pseudospin-1 Dirac-Weyl system with chaotic ray scattering dynamics from a stadium-shaped electrostatic-potential barrier in the Klein tunneling regime. (a) Super-Klein tunneling with omnidirectional and perfect transmission for the particle through a single straight potential step, where the incident wave energy is half of the potential height. (b) Stationary ray pattern inside the stadium barrier generated by reflections at the inner boundary. Due to Klein tunneling, the effective refractive index of the barrier is negative. Parallel ray paths are incident from the top of the stadium (one marked in blue), which correspond to a plane spinor wave in the short wavelength limit (upper panel). Lower panel: The result from full wave simulation, represented by the color-coded probability density distribution (in scale of its fourth root). (c) Quantitative test of ray-wave correspondence using the  $Y$ -dependent profile of the integral amplitude intensity over the horizontal range of the shaded region in the lower panel of (b), where the quantum and classical results are obtained from full wave simulation and the corresponding semiclassical ray model, respectively. (d)–(f) Results from the pseudospin-1/2 Dirac-Weyl scattering system with the same parameter setting for comparison. Parameters are  $a/R = 1$ , incident wave number  $kR = 300$ , and barrier height  $V_0 = 600 \hbar v_F/R$ .

line), respectively. The sharp resonances are a manifestation of the algebraic decay of the classical survival probability  $P(t)$ , as shown in Fig. 2(c) (dashed-orange and solid-gray lines). For either type of particles, the decay law is obtained from ray simulation that takes into account Klein tunneling. When there is classical chaos, for pseudospin-1/2 particles the sharp resonances have mostly disappeared [the green curve in Fig. 2(a)] but some resonances located at  $E \sim 50$  (i.e.,  $2\pi R/\lambda \sim 50$ ) persist for pseudospin-1 particles [the red curve in Fig. 2(b) and inset] in spite of a faster particle decay due to super-Klein tunneling from ray simulation [insets of Fig. 2(c)]. Representative distributions of LDOS patterns and local current vectors  $\mathbf{u}(\mathbf{r}) = v_F \Psi^\dagger(\mathbf{r}) \hat{\mathbf{S}} \Psi(\mathbf{r})$  for one such mode [specified by the cyan diamond marker in Fig. 2(b)], are

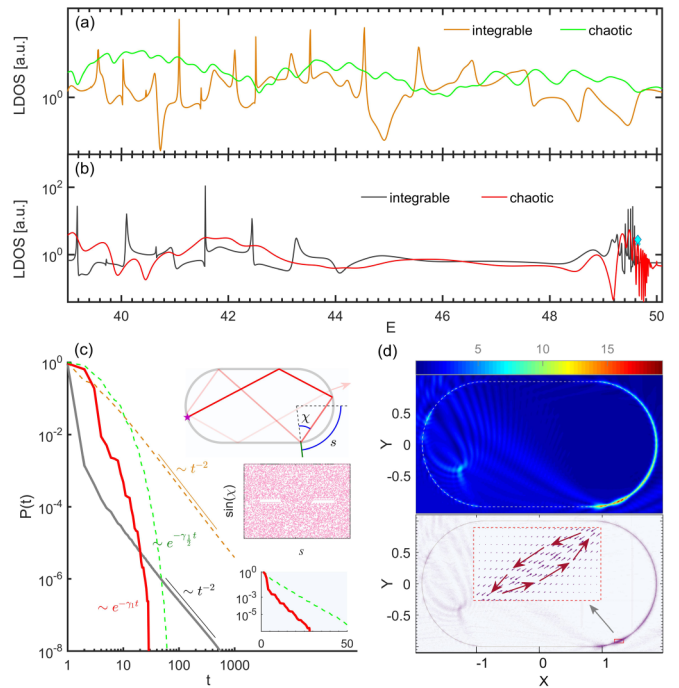


FIG. 2. Unique relativistic type of underbarrier scattering resonances against super-Klein tunneling which survive classical chaos. LDOS at a given position inside the potential barrier of height  $V_0 = 100$  (in units of  $\hbar v_F/R$ ) as a function of energy  $E$  ( $\hbar v_F/R$ ) for (a) pseudospin-1/2 and (b) pseudospin-1 systems, where two representative barrier shapes, a circle ( $a/R = 0$  - integrable) and a stadium ( $a/R = \sqrt{3}/2$  - chaotic), are used. (c) Semiclassical decay of the dwell time probability  $P(t)$  (scaled by the ray-tracing trajectory length) for pseudospin-1 (thick solid lines) and pseudospin-1/2 (thin dashed lines) particles. For classically integrable or chaotic dynamics, the decay is algebraic (solid-gray and dashed-orange lines) or exponential (solid-red and dashed-green lines), respectively. The insets show the shape of the electrostatic potential barrier, inside which a typical ray path starting from an arbitrary position on the boundary (indicated by a purple pentagram marker) is formed via successive amplitude loss at boundary reflections due to Klein tunneling (top), the related ergodic ray dynamics on the Poincaré surface of section (middle), and semi logarithmic plot of the resulting survival probability time distribution (bottom). (d) Upper panel: Typical real space probability density (on a square root scale) pattern of the edge mode as indicated by the cyan diamond marker in (b); lower panel: the associated local current density distribution with the formation of peculiar succession vortices strongly squeezed about a particular portion of the boundary (inset).

shown in Fig. 2(d). We see that, associated with this mode, particles are trapped locally near the boundary by strongly squeezed current vortices formed there. At a given resonant frequency, depending on the direction of the “illuminating” wave, its profile can change dramatically, e.g., from a connected one to two split ones with the chaotic cavity shape considered while the feature of peculiar edge localization persists. Remarkably, the cavity boundary harboring the localized edge excitations separates domains of a massless particle with approximately identical wavelength but opposite chirality, which is thus highly penetrable due to super-Klein tunneling in the absence of any external anti-Klein tunneling mechanisms of a

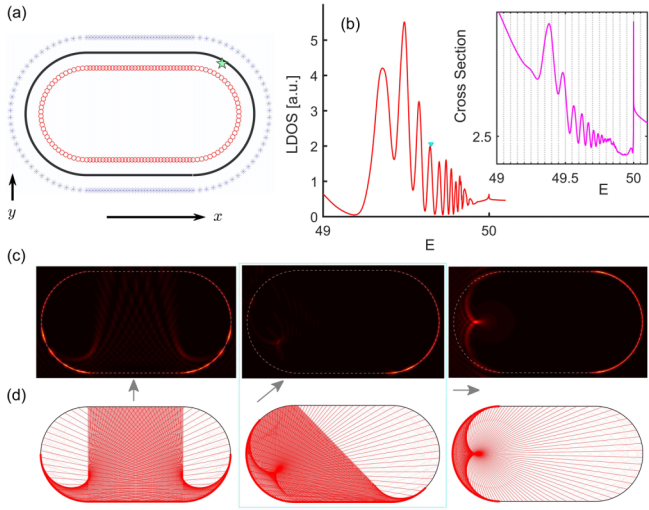


FIG. 3. Profiles of high  $Q$ , edge resonant modes that defy chaos and super-Klein tunneling. (a) The scatterer geometry where the blue stars and red circles denote the positions of multipoles or “fictitious” sources. (b) Numerical results of LDOS from our method with an inset showing the corresponding scattering cross section. (c) Spatial patterns of the edge mode for the specific energy value marked in (b) versus the direction of the incident wave indicated by the gray arrows. (d) The semiclassical counterparts. Parameters are  $a/R = \sqrt{3}/2$  and  $V_0 = 100 \hbar v_F / R$ .

magnetic field or gap-opening perturbations. The occurrence of the edge modes requires the creation of vortices near the boundary dominantly and can be attained in a narrow energy window [75]. Note that super-Klein tunneling enables massless spin-1 particles to pass through the boundary unimpeded at arbitrary incidence angles. The edge modes are capable of configuring the tangent/transverse component of the local current/spin density reversely across the boundary without degrading the magnitude. Dominant edge current and spin vortices can thus emerge at the boundary without translational invariance, which are responsible for the peculiar localized edge states in an ordered arrangement. Strikingly, the strong confinement persists in the presence of fully chaotic dynamics even in the relatively small wavelength limit, defying the semiclassical expectations.

### B. Controllable morphology of the emergent resonance modes

The spatial profiles of edge resonant modes that survive chaos and defy  $Q$ -spoiling can be controlled by changing the incident direction of the “illuminating” wave, as shown in Fig. 3. Especially, Fig. 3(a) shows the stadium geometry where the positions of multipoles or “fictitious” sources are indicated (the blue stars and red circles). Figure 3(b) and its inset show the LDOS and the scattering cross section versus the energy. Several spatial patterns of a typical resonant edge mode are shown in Fig. 3(c). The pseudospin, which is locked to momentum and hence the incident direction, can in general be regarded as being analogous to light polarization. This correspondence indicates that the surface resonant modes in pseudospin-1 systems uncovered here mimic the localized edge resonance modes in deformed metal nanoparticles [84].

Moreover, the emergence of the edge resonant modes contradicts the intuitive, semiclassical-based thinking that, in the presence of super-Klein tunneling, the chaotic (stadium) cavity is effectively a transparent superlens, as shown in Fig. 3(d).

## IV. SCATTERING OF PSEUDOSPIN-1 PARTICLES FROM NONINTEGRABLE CAVITIES OF AN ECCENTRIC ANNULAR POTENTIAL STEP

To demonstrate the peculiar cavity edge modes and their immunity to chaos more generally, we consider scattering of pseudospin-1 particles from an annular potential barrier, in which the degree of classical chaos can be systematically adjusted by varying the eccentricity parameter  $\xi$ . For this system, quantum scattering can be solved using the analytic scattering ( $S$ ) matrix formalism developed for pseudospin-1 Dirac-Weyl systems.

### A. S-matrix formulation

For the nonintegrable potential step with the eccentric annular shape, the scattering matrix can be obtained analytically through the techniques of wave-function matching and coordinate transformations, which were previously developed for scalar wave scattering in nonrelativistic quantum systems [85–87]. Here we extend the method to generalized pseudospin-1 wave scattering.

The required algebraic derivations are lengthy and more complicated than those for scalar or pseudospin-1/2 wave systems, as detailed in Appendix B. Here we list the main results in terms of formulas for the key quantities characterizing the quantum scattering. In particular, given that the potential shape is defined by two disks of different radii ( $R_1$  and  $R_2 < R_1$ ) with a finite relative displacement  $\xi$  between the disk centers, the resulting  $S$  matrix is given by

$$S = -\frac{\mathbb{Z}^{(2)} - \mathbb{Y}^{(2)} - s_{I\Pi} \mathbb{X}^{(2)} \mathbb{T}}{\mathbb{Z}^{(1)} - \mathbb{Y}^{(1)} - s_{I\Pi} \mathbb{X}^{(1)} \mathbb{T}}, \quad (6)$$

where  $s_{I\Pi}$  denote the band indices in the corresponding regions,  $\mathbb{T} = \mathbb{F}^{-1}(\mathbb{H} - \mathbb{G})$  with the conventions  $\mathbb{F} = \mathbf{x}^{(2)} + S^{od} \mathbf{x}^{(1)}$ ,  $\mathbb{G} = \mathbf{y}^{(2)} + S^{od} \mathbf{y}^{(1)}$ ,  $\mathbb{H} = \mathbf{z}^{(2)} + S^{od} \mathbf{z}^{(1)}$ ,

$$\begin{cases} \mathbb{X}^{(1,2)} = [H_m^{(1,2)}(k_0 R_1) \delta_{mj}], \\ \mathbb{Y}^{(1,2)} = [H_{m+1}^{(1,2)}(k_0 R_1) \delta_{mj}], \\ \mathbb{Z}^{(1,2)} = [H_{m-1}^{(1,2)}(k_0 R_1) \delta_{mj}], \end{cases} \quad (7)$$

$$\begin{cases} \mathbf{x}^{(1,2)} = [H_m^{(1,2)}(k_1 R_1) \delta_{mj}], \\ \mathbf{y}^{(1,2)} = [H_{m+1}^{(1,2)}(k_1 R_1) \delta_{mj}], \\ \mathbf{z}^{(1,2)} = [H_{m-1}^{(1,2)}(k_1 R_1) \delta_{mj}], \end{cases} \quad (8)$$

and

$$S^{od} = [J_{m-l}(k_1 \xi)] [S_l^{cd} \delta_{ll'}] [J_{m-l}(k_1 \xi)], \quad (9)$$

with

$$S_l^{cd} = -\frac{S_l^{cd-T}}{S_l^{cd-B}} \quad (10)$$

and

$$\begin{cases} S_I^{cd-T} \equiv J_I(k_{\text{III}}R_2)(H_{I-1}^{(2)}(k_{\text{II}}R_2) - H_{I+1}^{(2)}(k_{\text{II}}R_2)) - s_{\text{II}s_{\text{III}}}H_I^{(2)}(k_{\text{II}}R_2)(J_{I-1}(k_{\text{III}}R_2) - J_{I+1}(k_{\text{III}}R_2)), \\ S_I^{cd-B} \equiv J_I(k_{\text{III}}R_2)(H_{I-1}^{(1)}(k_{\text{II}}R_2) - H_{I+1}^{(1)}(k_{\text{II}}R_2)) - s_{\text{II}s_{\text{III}}}H_I^{(1)}(k_{\text{II}}R_2)(J_{I-1}(k_{\text{III}}R_2) - J_{I+1}(k_{\text{III}}R_2)). \end{cases} \quad (11)$$

### B. Edge-resonant modes that defy chaos $Q$ -spoiling and Klein tunneling

The confinement quality can be characterized by the Wigner-Smith time delay, which can be obtained from the  $S$  matrix as  $\tau(E) = -i\hbar\text{Tr}[S^\dagger\partial S/\partial E]$ . Sharp resonances with energy and thus strong confinement correspond to large positive values of  $\tau$ . Figures 4(a) and 4(b) show the dimensionless time delay versus  $\xi$  and particle energy  $E$  for pseudospin-1 and pseudospin-1/2 systems, respectively. For the former, there exists a particular set [red curves in Fig. 4(a)] where the time delay retains high values and is unaffected when the corresponding classical system becomes increasingly more chaotic. The quality factor of a cavity mode at energy  $E_n$

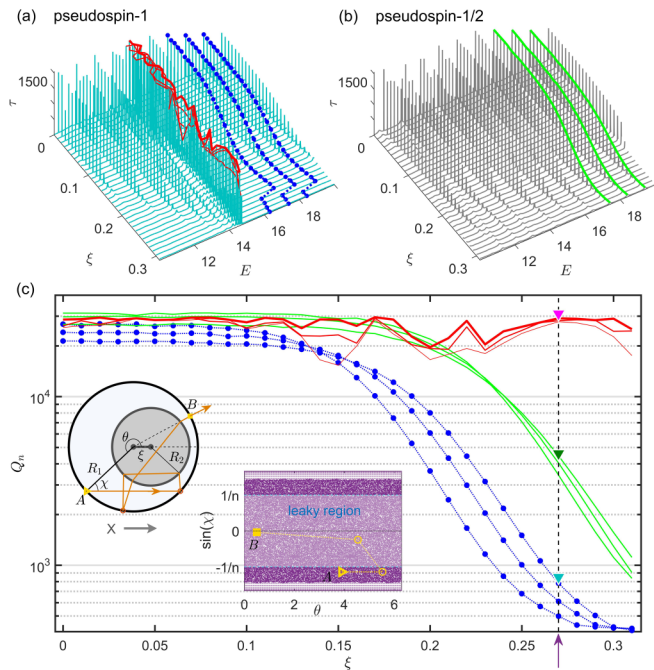


FIG. 4. Superconfinement in a chaotic scattering system of annular potential barrier. The degree of chaos can be controlled by the eccentric deformation parameter  $\xi$ . The characterizing quantities are obtained from a scattering matrix based analysis. (a), (b) Dimensionless Wigner-Smith time delay versus  $\xi$  (in units of  $R_1$ ) and particle energy  $E$  (in units of  $\hbar v_F/R_1$ ) for (a) pseudospin-1 and (b) pseudospin-1/2 systems, respectively. (c) Dependence of the  $Q$  factor of the representative modes marked in (a) and (b) on  $\xi$ . The left inset shows the shape of the potential barrier, inside which one typical ray trajectory (orange) initially undergoes total internal reflections and escapes from the barrier completely via Klein tunneling after a few collisions with perpendicular incidence at the outer boundary. Right inset: Chaos-rendered ergodic ray motion in the corresponding Poincaré surface of section. Other parameters are  $R_2/R_1 = 0.6$ , the potentials in the annular and inner disk regions are  $V_{\text{II}} = -10$  and  $V_{\text{III}} = 40$ , respectively.

is given by [88]  $Q_n = (E_n/\hbar)\tau(E_n)$ . For  $\xi = 0$  (integrable dynamics), a large number of high- $Q$  modes exist [highlighted by red, blue, and green colors in Figs. 4(a) and 4(b)]. The values of their quality factors versus  $\xi$  is shown in Fig. 4(c). Conventional wisdom stipulates that severe  $Q$ -spoiling would occur as the value of the deformation parameter is increased due to chaos-assisted tunneling [schematically illustrated in inset of Fig. 4(c)]. We see that the conventional wisdom holds, but only for the pseudospin-1/2 scattering system and for some states of the pseudospin-1 system, but, for the latter, there is a particular set of high- $Q$  modes that are completely immune to classical chaos. As the system and solution methods here are completely different from those for the stadium system, the results in Fig. 4 represent independent confirmation of the emergence of high- $Q$  cavity edge modes that defy chaos and Klein tunneling. A plausible physical origin of the robustness of these modes is spin-momentum locking, which can be elucidated by analyzing the transverse spin as done in a recent work on the quantum spin Hall effect of light [89].

### C. Spatial profiles of edge modes

Figure 4 presents the results of scattering of pseudospin-1 wave by an annular potential barrier. Here we provide the exact wave-calculation result, as shown in Fig. 5, where the red modes are localized edge modes, which can occur at either the inner or outer boundaries of the ring domain. For the given parameter values illustrated, they are confined at the inner boundary of the ring geometry. This is because, in this case, the required condition of sign change in the band indices rendering the edge modes arises only across the inner boundary. In Fig. 5, representative patterns for the conventional modes are also included (middle and right panels) for comparison,

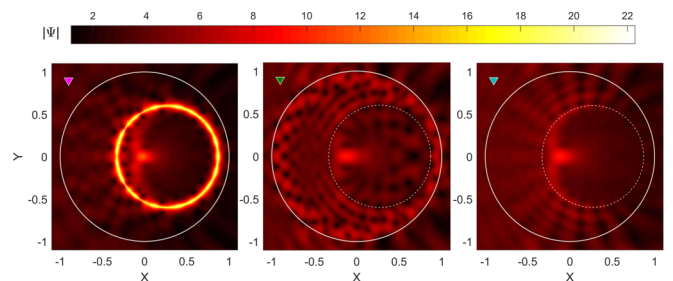


FIG. 5. Exactly calculated spatial profiles of representative resonant modes in pseudospin-1 and pseudospin-1/2 wave scattering. The modes are indicated by the corresponding colored triangles in Fig. 4(c). Left panel: A confined surface resonant mode in pseudospin-1 wave scattering. Middle panel: A conventional mode in pseudospin-1/2 wave scattering. Right panel: A conventional mode in pseudospin-1 scattering.

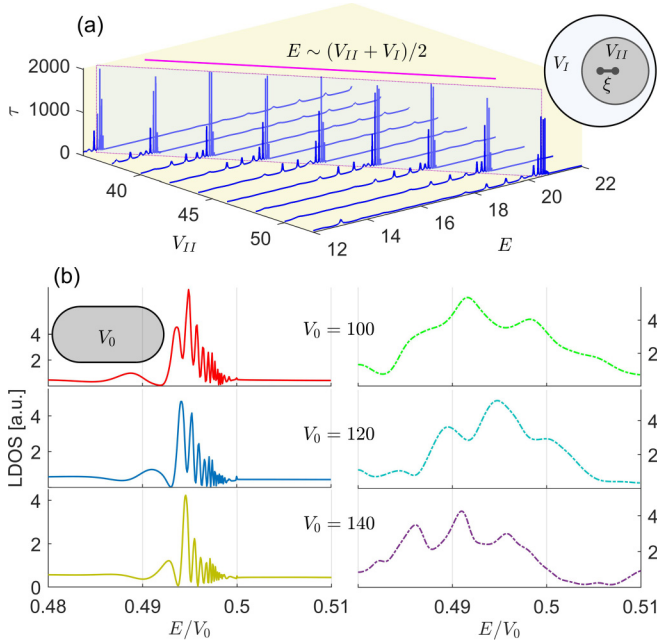


FIG. 6. Energy window for edge resonant modes that defy chaos  $Q$ -spoiling and Klein tunneling with respect to the external electrostatic potential. (a) Resonant modes in the energy domain versus the value of  $V_{II}$  for a strongly deformed annular barrier for  $\xi = 0.27$ ,  $R_2/R_1 = 0.6$ , and  $V_I = -10$ . (b) Edge modes in the chaotic stadium barrier ( $a/R = \sqrt{3}/2$ ) for pseudospin-1 (left column) and pseudospin-1/2 (right column) systems.

the confinement quality of which is typically destroyed by classical chaos.

## V. ENERGY WINDOW FOR EDGE RESONANT MODES

In the energy domain, the edge resonant modes associated with pseudospin-1 wave scattering occur in a quite predictable way in that the locations depend linearly on the applied potential, as shown in Figs. 6(a) and 6(b) for both types of chaotic systems studied. There is, in fact, a tunable energy window in which the modes can arise—a great advantage from the point of view of experimental observation. We emphasize that no such resonances are possible for pseudospin-1/2 particles.

We note that the presence of strong confinement does not necessarily correspond to peaks in the plot of LDOS defined at a given position versus the energy. The confinement, however, will have its manifestation of dramatic variances/changes in LDOS over a small energy interval, which would generically appear as peaks within a relatively large energy range. Examples of such peaks are shown in Fig. 2. In fact, the correspondence between peaks in LDOS and the cross section is indicative of strong confinement but becomes poor for weak confinement. The correspondence also depends on the specific position chosen. While, in principle, it is necessary to calculate the total DOS—a computationally demanding task, in practice (e.g., in an experiment), one can choose a proper position according to the pertinent parameters such as the particle energy and potential height. For example, when the energy and potential height are large, higher angular-momentum channels will be excited. In this case,

choosing the position near the cavity/scatterer boundary suffices.

## VI. DISCUSSION

The phenomenon of  $Q$ -spoiling by ray (classical) chaos has been known in optics for more than two decades [9–11]. In electronic transport through a quantum dot, chaos can remove the sharp resonances associated with conductance fluctuations, which would occur if the classical dynamics were integrable [12–19]. We have uncovered a quantum chaotic scattering paradox/anomaly for massless spin-1 particles: In a relevant short-wavelength regime, high- $Q$  (resonance) trapping persists in leaking chaotic cavities with a super-Klein tunneling enabled transparent boundary, contradicting the semiclassical expectations. This presents a remarkable exception to the conventional wisdom that wave trapping would be impossible in the simultaneous presence of chaos and Klein tunneling: Not only do the modes defy chaos  $Q$ -spoiling, they are also immune to super-Klein tunneling. This finding is relevant to the fields of optics, solid state physics, and quantum chaos, with potential applications in 2D Dirac-Weyl material and photonic systems.

An experimental test of the phenomenon uncovered in this paper is feasible through, e.g., two-dimensional electronic Lieb lattices that have been realized recently [49,50]. A concrete link with experiments is as follows. To verify the existence of edge resonant modes in pseudospin-1 wave scattering, a viable experimental setting is transport in electronic Lieb lattice systems. In a typical transport and conductance-probe setup with a quantum dot and waveguide geometry, resonant scattering occurs naturally [90]. The interference between the waveguiding channels (instead of simple unbounded plane waves) and individual cavity resonant (quasibound) modes will give rise to intricate Fano patterns that appear as asymmetric dips and peaks on top of the background conductance plateau. The presence of long-lived surface cavity modes would have their fingerprints as robust and sharp conductance fluctuations in the energy regime of Klein tunneling, regardless of classical chaos.

We make a number of remarks pertinent to the finding of this paper.

*Remark 1.* Results in this paper that go beyond those in our previous work. In Ref. [75], we studied scattering of pseudospin-1 particles from a circular potential domain, derived boundary conditions for the Dirac-Weyl equation, obtained analytic formulas for various scattering cross sections, and found a class of resonant modes that are trapped near the boundary inside the potential region. From a classical point of view, the dynamics in a circular domain are integrable and there are stable periodic orbits inside the scattering region. As such, the emergence of long-lived, sharp resonant modes in the quantum regime is not surprising. A question that is fundamental to the field of quantum chaos, which we were not able to answer at that time, was whether these modes can persist when the domain is deformed so there is fully developed chaos in the classical limit. The difficulty lies in the lack of even numerical methods to calculate the scattering wave functions for the three-component spinor

when the potential domain is deformed from the circular shape.

According to wisdom from microcavity optics [9–11] and mesoscopic transport physics [12–19], when the classical dynamics are fully chaotic, long-lived resonant modes are unlikely, which is the well-known phenomenon of  $Q$ -spoiling. Intuitively, the expectations were that pseudospin-1 chaotic scattering ought to behave in a similar way. Our development of the multiple multipole method has enabled us to study pseudospin-1 wave scattering in arbitrary potential domain, as detailed in the present paper. What has been found, to our surprise, is that pseudospin-1 particles can still be trapped inside the potential domain through the long-lived resonant modes, regardless of the boundary deformations—even those that lead to fully developed chaos in the classical limit. More surprisingly, in the energy regime studied, pseudospin-1 particles exhibit super-Klein tunneling, which would make trapping even more unlikely. The emergence of the resonant boundary trapping modes thus defies all existing understanding of the interplay among classical chaos, trapping, and Klein tunneling. The phenomenon reported in the current paper is thus fundamental to at least three areas in physics: quantum chaos, microlasing optics, and mesoscopic or nanotransport in two-dimensional solid state systems, representing an advance going far beyond the results in Ref. [75].

*Remark 2.* Persistence of long-lived boundary trapping modes in the semiclassical, short-wavelength regime. There was previous work discussing the persistent effect of classical chaos in the deep quantum (long wavelength) regime [91,92]. This was counterintuitive because the quantum manifestations of chaos occur typically in the semiclassical (short wavelength) regime. What we have found here is somewhat opposite: Long-lived resonant modes, typically a quantum behavior in the long wavelength regime, persist in the semiclassical regime and completely defy classical chaos, leading to a breakdown of the quantum-classical correspondence. A plausible reason lies in the three-component spinor wavefunction structure of pseudospin-1 particles, where the boundary conditions are drastically different from those for scalar or even two-component spinor wave functions [75]. Especially, at the boundary of the potential domain, two quantities must be continuous: (1) the second (middle) spinor component and (2) the algebraic sum of the phase modulated first and third spinor components. Mathematically, the boundary conditions mean that one of the spinor components can have an arbitrary finite value. There are thus significantly more possibilities to configure the distribution of the resulting wave density and the corresponding local current density than for scalar wave and spin-1/2 Dirac wave. A remarkable consequence is the formation of vortexlike boundary trapping modes, which was analytically demonstrated by using the Mie theory for pseudospin-1 wave for the case of an integrable circular cavity [75]. For chaotic cavities, an analytic theory is not feasible. Nonetheless, as we have demonstrated in this paper, the wave-coherence-based boundary trapping modes persist, regardless of the chaos rendered irregularities and/or randomness. Unlike the conventional whispering gallery modes and scars associated with a chaotic cavity for scalar or pseudospin-1/2 waves, the boundary trapping modes for pseudospin-1 waves have no classical correspondence. The particular localization

feature of these modes is due to the nonintegrable cavity geometry that breaks the circularly rotational symmetry. Depending on the direction of the incident wave, e.g., whether it is along the axis of symmetry of the cavity or not, the locations where these localized states occur are different.

*Remark 3.* Need to study the classical-quantum correspondence in systems described by multicomponent spinor wave functions. Most previous discussions of the classical-quantum correspondence in the literature were for the scalar wave function described by the Schrödinger equation. The breakdown of the classical-quantum correspondence uncovered in this paper owes its origin to the three-component structure of the spinor wave function for pseudospin-1 particles. As a fundamental issue in physics, the classical-quantum correspondence in systems described by multicomponent wave functions should be examined more deliberately, as the “classical” equation of motion may be different from the one in spinless systems [93,94].

## ACKNOWLEDGMENT

We would like to acknowledge support from the Vannevar Bush Faculty Fellowship program sponsored by the Basic Research Office of the Assistant Secretary of Defense for Research and Engineering and funded by the Office of Naval Research through Grant No. N00014-16-1-2828.

## APPENDIX A: MULTIPLE MULTIPOLES METHOD FOR RELATIVISTIC QUANTUM SCATTERING OF PSEUDOSPIN-1 WAVE

### 1. Implementation

For simplicity but without loss of generality, we develop the multiple multipoles method based on the concrete setting of a single potential step of arbitrary shape. This leads to two subregions denoted by I and II, as shown in Fig. 7. The generalized Dirac-Weyl equation in each subregion  $\tau \in \{I, II\}$  reads

$$\hat{S} \cdot \hat{\mathbf{k}} \Psi^{(\tau)}(\mathbf{r}) = \epsilon_{\tau} \Psi^{(\tau)}(\mathbf{r}), \quad (\text{A1})$$

where  $\epsilon_{\tau} = (E - V_{\tau})/\hbar v_F$ . In the polar coordinates  $\mathbf{r} = (r, \theta)$ , the spinor cylindrical wave basis of solutions with angular momentum  $l$  is

$$\Psi_l^{(\tau)}(\mathbf{r}) = \begin{pmatrix} B_{l-1}(k_{\tau} r) e^{-i\theta} \\ i s_{\tau} B_l(k_{\tau} r) \\ -B_{l+1}(k_{\tau} r) e^{i\theta} \end{pmatrix} e^{il\theta}, \quad (\text{A2})$$

where  $s_{\tau} = \text{sgn}(E - V_{\tau})$  denotes the relevant band index and  $k_{\tau} = |E - V_{\tau}|/\hbar v_F$ . Assuming  $E > 0$  and choosing  $B_l(k_{\tau} r) = H_l^{(1)}(k_{\tau} r)$  (with  $H_l^{(1)}$  being the Hankel function of the first kind), we define the Dirac-type wave functions of multipoles outside the specific solving region  $\tau$  and positioned at  $\mathbf{r}_{m_{\bar{\tau}}}$  as

$$\Psi_l^{(\tau)}(\mathbf{d}_{m_{\bar{\tau}}}) = \frac{1}{\sqrt{2}} \begin{pmatrix} H_{l-1}^{(1)}(k_{\tau} d_{m_{\bar{\tau}}}) e^{-i\theta_{m_{\bar{\tau}}}} \\ i\sqrt{2} s_{\tau} H_l^{(1)}(k_{\tau} d_{m_{\bar{\tau}}}) \\ -H_{l+1}^{(1)}(k_{\tau} d_{m_{\bar{\tau}}}) e^{i\theta_{m_{\bar{\tau}}}} \end{pmatrix} e^{il\theta_{m_{\bar{\tau}}}}, \quad (\text{A3})$$

where  $\bar{\tau}$  denotes the complement of  $\tau$ ,  $d_{m_{\bar{\tau}}} \equiv |\mathbf{d}_{m_{\bar{\tau}}}| = |\mathbf{r} - \mathbf{r}_{m_{\bar{\tau}}}|$  and  $\theta_{m_{\bar{\tau}}} = \text{Angle}(\mathbf{r} - \mathbf{r}_{m_{\bar{\tau}}})$  with  $\mathbf{r} \in \tau$ . Carrying out



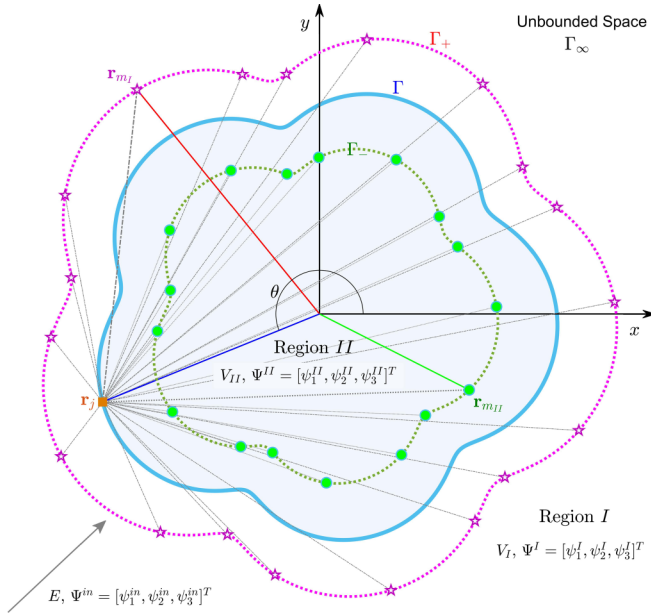


FIG. 7. Schematic illustration of scattering problem to be solved:  $\Gamma$  is the physical boundary separating regions II and I, while  $\Gamma_{\pm}$  are auxiliary boundaries at which the multiple multipoles (“fictitious” sources) are placed with coordinates denoted by  $\mathbf{r}_{m_I}$  and  $\mathbf{r}_{m_{II}}$ . The sources at  $\Gamma_{-}$  (green circular dots) radiate the pseudospin-1 field  $\Psi_I^l(\mathbf{r} - \mathbf{r}_{m_I})$  used to determine the wave function in region I, while the ones at  $\Gamma_{+}$  (pentagrams) generate the field  $\Psi_{II}^l(\mathbf{r} - \mathbf{r}_{m_{II}})$  used to determine the wave function in region II. Boundary conditions are satisfied at the collocation points  $\mathbf{r}_j \in \Gamma$ .

multiple multipoles expansion for the specific region, we obtain the wave function in region II as

$$\begin{aligned} \Psi^{(II)}(\mathbf{r}) &= \sum_{m_{II}} \sum_l C_l^{m_{II}} \frac{1}{\sqrt{2}} \begin{pmatrix} H_{l-1}^{(1)}(k_{II}d_{m_{II}})e^{-i\theta_{m_{II}}} \\ i\sqrt{2}s_{II}H_l^{(1)}(k_{II}d_{m_{II}}) \\ -H_{l+1}^{(1)}(k_{II}d_{m_{II}})e^{i\theta_{m_{II}}} \end{pmatrix} e^{il\theta_{m_{II}}} \\ &\equiv \begin{pmatrix} \psi_1^{II} \\ \psi_2^{II} \\ \psi_3^{II} \end{pmatrix}. \end{aligned} \quad (\text{A4})$$

The scattered (outgoing) wave function in region I has the form

$$\begin{aligned} \Psi^{(I)}(\mathbf{r}) &= \sum_{m_I} \sum_l C_l^{m_I} \frac{1}{\sqrt{2}} \begin{pmatrix} H_{l-1}^{(1)}(k_I d_{m_I})e^{-i\theta_{m_I}} \\ i\sqrt{2}s_I H_l^{(1)}(k_I d_{m_I}) \\ -H_{l+1}^{(1)}(k_I d_{m_I})e^{i\theta_{m_I}} \end{pmatrix} e^{il\theta_{m_I}} \\ &\equiv \begin{pmatrix} \psi_1^I \\ \psi_2^I \\ \psi_3^I \end{pmatrix}. \end{aligned} \quad (\text{A5})$$

A planar incident wave propagating along the direction that makes an angle  $\beta$  with the  $x$  axis in region I can be

written as

$$\Psi^{\text{in}}(\mathbf{r}) = \frac{1}{2} \begin{pmatrix} e^{-i\beta} \\ \sqrt{2}s_I \\ e^{i\beta} \end{pmatrix} e^{ik \cdot \mathbf{r}} = \begin{pmatrix} \psi_1^{\text{in}} \\ \psi_2^{\text{in}} \\ \psi_3^{\text{in}} \end{pmatrix}. \quad (\text{A6})$$

Imposing the relevant boundary conditions parameterized by the angle  $\alpha$  between the outward normal at any boundary point  $\mathbf{r}_j$  and the  $x$  axis,

$$(\psi_2^{(I)} + \psi_2^{\text{in}})|_{\mathbf{r}_j \in \Gamma} = \psi_2^{(II)}|_{\mathbf{r}_j \in \Gamma}, \quad (\text{A7})$$

$$\begin{aligned} &([\psi_1^{(I)} + \psi_1^{\text{in}}]e^{i\alpha} + [\psi_3^{(I)} + \psi_3^{\text{in}}]e^{-i\alpha})|_{\mathbf{r}_j \in \Gamma} \\ &= (\psi_1^{(II)}e^{i\alpha} + \psi_3^{(II)}e^{-i\alpha})|_{\mathbf{r}_j \in \Gamma}, \end{aligned} \quad (\text{A8})$$

we obtain

$$\sum_{m_{II}} \sum_l {}^j A_{lm_{II}}^{(I)} C_l^{m_{II}} - \sum_{m_I} \sum_l {}^j A_{lm_I}^{(II)} C_l^{m_I} = -j \psi_2^{\text{in}}, \quad (\text{A9a})$$

$$\sum_{m_{II}} \sum_l {}^j B_{lm_{II}}^{(I)} C_l^{m_{II}} - \sum_{m_I} \sum_l {}^j B_{lm_I}^{(II)} C_l^{m_I} = -j \chi^{\text{in}}, \quad (\text{A9b})$$

where the substitutions are given by

$${}^j A_{lm_{II}}^{(I)} = i s_I H_l^{(1)}(k_I |\mathbf{r}_j - \mathbf{r}_{m_{II}}|) e^{il\theta_{m_{II}}}, \quad (\text{A10a})$$

$${}^j A_{lm_I}^{(II)} = i s_{II} H_l^{(1)}(k_{II} |\mathbf{r}_j - \mathbf{r}_{m_I}|) e^{il\theta_{m_I}}, \quad (\text{A10b})$$

$$\begin{aligned} {}^j B_{lm_{II}}^{(I)} &= \frac{1}{\sqrt{2}} [H_{l-1}^{(1)}(k_I |\mathbf{r}_j - \mathbf{r}_{m_{II}}|) e^{i(l-1)\theta_{m_{II}}} e^{i\alpha} \\ &\quad - H_{l+1}^{(1)}(k_I |\mathbf{r}_j - \mathbf{r}_{m_{II}}|) e^{i(l+1)\theta_{m_{II}}} e^{-i\alpha}], \end{aligned} \quad (\text{A10c})$$

$$\begin{aligned} {}^j B_{lm_I}^{(II)} &= \frac{1}{\sqrt{2}} [H_{l-1}^{(1)}(k_{II} |\mathbf{r}_j - \mathbf{r}_{m_I}|) e^{i(l-1)\theta_{m_I}} e^{i\alpha} \\ &\quad - H_{l+1}^{(1)}(k_{II} |\mathbf{r}_j - \mathbf{r}_{m_I}|) e^{i(l+1)\theta_{m_I}} e^{-i\alpha}], \end{aligned} \quad (\text{A10d})$$

and

$${}^j \psi_2^{\text{in}} = \frac{1}{\sqrt{2}} s_I e^{ik_I \cdot \mathbf{r}_j}, \quad (\text{A10e})$$

$${}^j \chi^{\text{in}} = \frac{1}{2} [e^{i(\alpha-\beta)} + e^{-i(\alpha-\beta)}] e^{ik_I \cdot \mathbf{r}_j}. \quad (\text{A10f})$$

In principle, the set consists of an infinite number of equations with an infinite number of undetermined expansion coefficients  $C_l^{m_{II}}$  and  $C_l^{m_I}$ . To solve the system numerically, a finite truncation is necessary, which turns out to be feasible in practice by discretizing the boundary to a finite number of points  $J$  and setting the number of multipoles  $M_{\tau}$  in the specific region  $\tau$  and  $l \in [-L, L]$  for all the multipoles. Carrying out the discretization procedure, we arrive at the following finite dimensional matrix equation:

$$\mathbb{M}_{2J \times N} \cdot \mathbf{C}_{N \times 1} = -\mathbf{Y}_{2J \times 1}, \quad (\text{A11})$$

where  $N = (2L + 1) \times (M_I + M_{II}) = N_I + N_{II}$  and the compact substitutions are

$$\mathbf{C}_{N \times 1} = \begin{pmatrix} C_{-L}^{1_{II}} \\ \vdots \\ C_l^{1_{II}} \\ C_l^{2_{II}} \\ \vdots \\ C_l^{M_{II}} \\ \vdots \\ C_L^{M_{II}} \\ \hline C_{-L}^{1_I} \\ \vdots \\ C_l^{1_I} \\ C_l^{2_I} \\ \vdots \\ C_l^{M_I} \\ \vdots \\ C_L^{M_I} \end{pmatrix}_{N \times 1} ; \quad \mathbf{Y}_{2J \times 1} = \begin{pmatrix} {}^1\psi_2^{\text{in}} \\ \vdots \\ {}^j\psi_2^{\text{in}} \\ \vdots \\ {}^J\psi_2^{\text{in}} \\ \hline {}^1\chi^{\text{in}} \\ \vdots \\ {}^j\chi^{\text{in}} \\ \vdots \\ {}^J\chi^{\text{in}} \end{pmatrix}_{2J \times 1} \tag{A12a}$$

and

$$\mathbb{M}_{2J \times N} = \left( \begin{array}{c|c} \mathbb{A}^{(I)} & -\mathbb{A}^{(II)} \\ \hline \mathbb{B}^{(I)} & -\mathbb{B}^{(II)} \end{array} \right)_{2J \times N}, \tag{A12b}$$

with

$$\mathbb{A}^{(\tau)} = \begin{pmatrix} {}^1A_{-L1\bar{\tau}}^{(\tau)} & \cdots & {}^1A_{l1\bar{\tau}}^{(\tau)} & {}^1A_{l2\bar{\tau}}^{(\tau)} & \cdots & {}^1A_{lM\bar{\tau}}^{(\tau)} & \cdots & {}^1A_{LM\bar{\tau}}^{(\tau)} \\ {}^2A_{-L1\bar{\tau}}^{(\tau)} & \cdots & {}^2A_{l1\bar{\tau}}^{(\tau)} & {}^2A_{l2\bar{\tau}}^{(\tau)} & \cdots & {}^2A_{lM\bar{\tau}}^{(\tau)} & \cdots & {}^2A_{LM\bar{\tau}}^{(\tau)} \\ \vdots & \cdots & \vdots & \vdots & \cdots & \vdots & \cdots & \vdots \\ {}^jA_{-L1\bar{\tau}}^{(\tau)} & \cdots & {}^jA_{l1\bar{\tau}}^{(\tau)} & {}^jA_{l2\bar{\tau}}^{(\tau)} & \cdots & {}^jA_{lM\bar{\tau}}^{(\tau)} & \cdots & {}^jA_{LM\bar{\tau}}^{(\tau)} \\ \vdots & \cdots & \vdots & \vdots & \cdots & \vdots & \cdots & \vdots \\ {}^JA_{-L1\bar{\tau}}^{(\tau)} & \cdots & {}^JA_{l1\bar{\tau}}^{(\tau)} & {}^JA_{l2\bar{\tau}}^{(\tau)} & \cdots & {}^JA_{lM\bar{\tau}}^{(\tau)} & \cdots & {}^JA_{LM\bar{\tau}}^{(\tau)} \end{pmatrix}_{J \times N_{\bar{\tau}}}, \tag{A12c}$$

$$\mathbb{B}^{(\tau)} = \begin{pmatrix} {}^1B_{-L1\bar{\tau}}^{(\tau)} & \cdots & {}^1B_{l1\bar{\tau}}^{(\tau)} & {}^1B_{l2\bar{\tau}}^{(\tau)} & \cdots & {}^1B_{lM\bar{\tau}}^{(\tau)} & \cdots & {}^1B_{LM\bar{\tau}}^{(\tau)} \\ {}^2B_{-L1\bar{\tau}}^{(\tau)} & \cdots & {}^2B_{l1\bar{\tau}}^{(\tau)} & {}^2B_{l2\bar{\tau}}^{(\tau)} & \cdots & {}^2B_{lM\bar{\tau}}^{(\tau)} & \cdots & {}^2B_{LM\bar{\tau}}^{(\tau)} \\ \vdots & \cdots & \vdots & \vdots & \cdots & \vdots & \cdots & \vdots \\ {}^jB_{-L1\bar{\tau}}^{(\tau)} & \cdots & {}^jB_{l1\bar{\tau}}^{(\tau)} & {}^jB_{l2\bar{\tau}}^{(\tau)} & \cdots & {}^jB_{lM\bar{\tau}}^{(\tau)} & \cdots & {}^jB_{LM\bar{\tau}}^{(\tau)} \\ \vdots & \cdots & \vdots & \vdots & \cdots & \vdots & \cdots & \vdots \\ {}^JB_{-L1\bar{\tau}}^{(\tau)} & \cdots & {}^JB_{l1\bar{\tau}}^{(\tau)} & {}^JB_{l2\bar{\tau}}^{(\tau)} & \cdots & {}^JB_{lM\bar{\tau}}^{(\tau)} & \cdots & {}^JB_{LM\bar{\tau}}^{(\tau)} \end{pmatrix}_{J \times N_{\bar{\tau}}}. \tag{A12d}$$

As the expansions are generally nonorthogonal, more equations are required than unknowns to enable deduction of an overdetermined matrix system with  $2J \gg N$ , which can be solved by the pseudoinverse algorithm (e.g., in Matlab):

$\mathbf{C} = -\text{pinv}(\mathbb{M}) * \mathbf{Y}$ . In particular, we use the residual error evaluated at the boundary

$$\text{SSE} = \frac{\|\mathbb{M} * \mathbf{C} + \mathbf{Y}\|}{\|\mathbf{Y}\|}$$

as the criterion for testing convergence. Especially, we adjust the number, the order and/or positions of the multipoles to ensure  $SSE < \text{tolerance}$ . After the unknown coefficients  $C$  have been obtained, the associated wave functions and hence the LDOS in the specific region can be calculated accordingly.

We can also calculate the characteristic cross section from the scattered wave function as given in Eq. (A5). Rewriting the wave function in terms of the position variables  $r$  and  $\theta$ , we have

$$\Psi^{(1)}(r, \theta) = \sum_{m_{\Pi}} \sum_l \frac{C_l^{m_{\Pi}}}{\sqrt{2}} \sum_n J_n(kr_{m_{\Pi}}) \times \begin{pmatrix} H_{l+n-1}^{(1)}(k_1 r) e^{-i\theta} \\ i\sqrt{2} s_1 H_{l+n}^{(1)}(k_1 r) \\ -H_{l+n+1}^{(1)}(k_1 r) e^{i\theta} \end{pmatrix} e^{i(l+n)\theta}. \quad (\text{A13})$$

In the far-field, i.e.,  $k_1 r \rightarrow \infty$ , we get

$$\Psi^{(1)}(r, \theta) \rightarrow \sum_{m_{\Pi}} \sum_l \sum_n \frac{\sqrt{2/\pi} k C_l^{m_{\Pi}} e^{i(l+n)\theta}}{i^{l+n} \sqrt{-ir}} \times J_n(kr_{m_{\Pi}}) \begin{pmatrix} e^{-i\theta} \\ i\sqrt{2} s_1 \\ e^{i\theta} \end{pmatrix}. \quad (\text{A14})$$

The far-field scattering amplitude can be obtained as

$$f(\theta) = \sqrt{\frac{2}{\pi k}} \sum_{m_{\Pi}} \sum_l \sum_n \frac{C_l^{m_{\Pi}} J_n(kr_{m_{\Pi}})}{i^{l+n}} e^{i(l+n)\theta}, \quad (\text{A15})$$

and associated cross section is given by

$$\sigma = \oint |f(\theta)|^2 d\theta. \quad (\text{A16})$$

## 2. Method validation

To validate our method, we make use of a classically integrable system for which the scattering characteristics can be obtained analytically by evaluating the scattering cross section according to the formula

$$\tilde{\sigma} = \frac{4}{k} \sum_l |\tilde{a}_l|^2, \quad (\text{A17a})$$

where

$$\tilde{a}_l = -\frac{\tilde{F}_l}{\tilde{F}_l + i\tilde{G}_l}, \quad (\text{A17b})$$

with

$$\begin{aligned} \tilde{F}_l &= J_l(\beta x) J_l'(x) - s_1 s_{\Pi} J_l'(\beta x) J_l(x), \\ \tilde{G}_l &= J_l(\beta x) Y_l'(x) - s_1 s_{\Pi} J_l'(\beta x) Y_l(x), \end{aligned}$$

and  $\beta = |E - V_0|/|E|$ .

Figure 8 shows a comparison of the typical scattering resonances obtained analytically and from the numerical method. There is a good agreement. In fact, there is a quite accurate correspondence between the peaks in the LDOS and in the cross section in the regime of strong confinement (the focus of our present paper), although the accuracy somewhat degrades

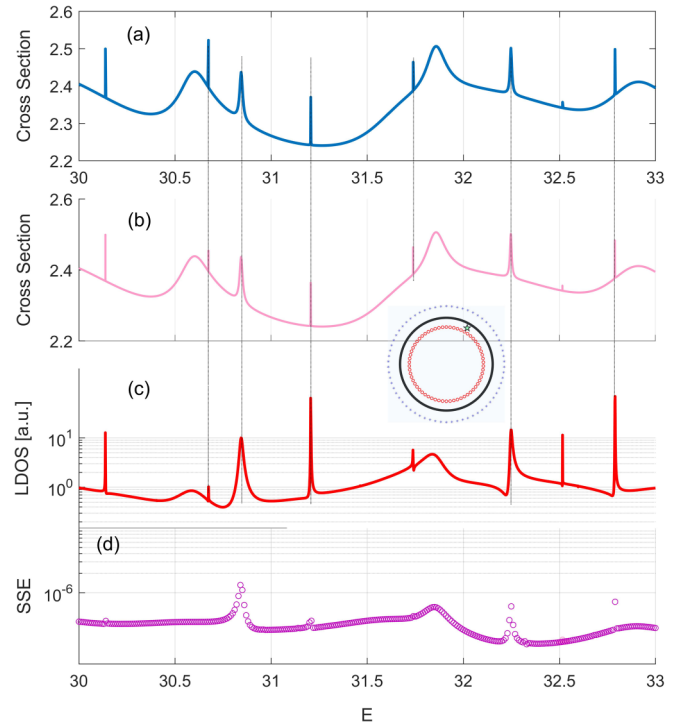


FIG. 8. Validation of the multiple multipoles method for a classically integrable scattering system. For pseudospin-1 waves, (a) scattering resonances versus energy characterized by the cross section obtained analytically from the partial wave decomposition method, (b) the cross section calculated from our multipole method, (c) scattering resonances characterized by the local density of states at a given position inside the barrier (indicated by the green pentagram in the inset), which are calculated numerically using the multiple multipoles method, and (d) the corresponding residual error versus energy characterizing the convergence of the multipole method. The potential height is  $V_0 = 100 \hbar v_F/R$ .

in the regime of weak confinement. In general, the effectiveness of using peaks in the LDOS as an indicator of strong confinement depends on the specific location to probe the LDOS pattern, where locations near the domain boundary are typically more effective. In practice (e.g., in an experimental situation), the position can be chosen properly according to the parameter values such as the particle energy and potential height. For example, when the values of both energy and potential height are relatively large, higher angular-momentum channels are excited. In this case, the best region to choose the position is near the cavity/scatterer boundary.

## APPENDIX B: S-MATRIX APPROACH TO PSEUDOSPIN-1 WAVE SCATTERING FROM NONINTEGRABLE CAVITIES OF AN ECCENTRIC ANNULAR POTENTIAL STEP

For a nonintegrable potential step with the eccentric annular shape, the scattering matrix can be obtained analytically through the techniques of wave-function matching and coordinate transformations, which were previously developed for scalar wave scattering in nonrelativistic quantum systems [85–87] and recently for relativistic quantum scattering of

massless spin-1/2 Dirac fermions [83]. Here we extend the method to generalized pseudospin-1 wave scattering.

Given that the potential shape is defined by two disks of different radii ( $R_1$  and  $R_2 < R_1$ ) with a finite relative displacement  $\xi$  between the disk centers, we use the convention that the global unprimed coordinates are defined by choosing the origin as the center of the larger disk  $O$  while the local primed ones have their origin sitting at the small disk center  $O'$ . Adopting the standard  $S$ -matrix formalism, in the unprimed polar coordinates  $\mathbf{r} = (r, \theta)$ , the wave function outside the eccentric annular scatterer, i.e.,  $|\mathbf{r}| > R_1$ , can be written as

$$\Psi^{(I)}(\mathbf{r}) = \sum_{m=-\infty}^{\infty} a_m^I \left[ k_I h_m^{(2)} + \sum_{m'=-\infty}^{\infty} S_{mm'}^{k_I} h_{m'}^{(1)} \right], \quad (\text{B1})$$

where

$$k_I h_m^{(1,2)} = \frac{1}{2} \begin{pmatrix} H_{m-1}^{(1,2)}(k_I r) e^{-i\theta} \\ i\sqrt{2} s_I H_m^{(1,2)}(k_I r) \\ H_{m+1}^{(1,2)}(k_I r) e^{i\theta} \end{pmatrix} e^{im\theta}$$

and  $S_{mm'}$  denotes the  $S$ -matrix elements in terms of two given channels indexed by  $m$  and  $m'$ , respectively, and the coefficient  $a_m^0$  is chosen to yield a desired kind of incident test wave. For

simplicity but without loss of generality, we set  $a_m^I \equiv 1$ . We thus have

$$\Psi^{(I)}(\mathbf{r}) = \sum_{m=-\infty}^{\infty} \left[ k_0 h_m^{(2)} + \sum_{m'=-\infty}^{\infty} S_{mm'}^{k_0} h_{m'}^{(1)} \right]. \quad (\text{B2})$$

The wave function in the annular region, i.e.,  $|\mathbf{r}'| > R_2$  and  $|\mathbf{r}'| < R_1$ , can be expressed in the primed coordinates  $\mathbf{r}' = (r', \theta')$  as

$$\tilde{\Psi}^{(II)}(\mathbf{r}') = \sum_{m=-\infty}^{\infty} \sum_{l=-\infty}^{\infty} m \tilde{a}_l^{II} \left[ k_{II} \tilde{h}_l^{(2)} + S_l^{cd} k_{II} \tilde{h}_l^{(1)} \right], \quad (\text{B3})$$

where

$$k_{II} \tilde{h}_l^{(1,2)} = \frac{1}{2} \begin{pmatrix} H_{l-1}^{(1,2)}(k_{II} r') e^{-i\theta'} \\ i\sqrt{2} s_{II} H_l^{(1,2)}(k_{II} r') \\ H_{l+1}^{(1,2)}(k_{II} r') e^{i\theta'} \end{pmatrix} e^{il\theta'}$$

and

$$S_l^{cd} = -\frac{S_l^{cd-T}}{S_l^{cd-B}} \quad (\text{B4})$$

with

$$\begin{cases} S_l^{cd-T} \equiv J_l(k_{III} R_2) (H_{l-1}^{(2)}(k_{II} R_2) - H_{l+1}^{(2)}(k_{II} R_2)) - s_{II} s_{III} H_l^{(2)}(k_{II} R_2) (J_{l-1}(k_{III} R_2) - J_{l+1}(k_{III} R_2)), \\ S_l^{cd-B} \equiv J_l(k_{III} R_2) (H_{l-1}^{(1)}(k_{II} R_2) - H_{l+1}^{(1)}(k_{II} R_2)) - s_{II} s_{III} H_l^{(1)}(k_{II} R_2) (J_{l-1}(k_{III} R_2) - J_{l+1}(k_{III} R_2)). \end{cases} \quad (\text{B5})$$

Making use of the Graf's addition theorem for Bessel functions,

$$H_l^{(1,2)}(kr') e^{il\theta'} = \sum_n J_n(k\xi) H_{l+n}(kr) e^{i(l+n)\theta},$$

we can rewrite Eq. (B3) as

$$\tilde{\Psi}^{(II)}(\mathbf{r}') = \sum_{m=-\infty}^{\infty} \sum_{l=-\infty}^{\infty} m \tilde{a}_l^{II} \left[ \sum_n J_n(k_{II} \xi) k_{II} h_{l+n}^{(2)} + S_l^{cd} \sum_n J_n(k_{II} \xi) k_{II} h_{l+n}^{(1)} \right]. \quad (\text{B6})$$

With the convention  $l+n \equiv \mu$ , we further have

$$\begin{aligned} \tilde{\Psi}^{(II)}(\mathbf{r}') &= \sum_{m=-\infty}^{\infty} \sum_{l=-\infty}^{\infty} m \tilde{a}_l^{II} \left[ \sum_{\mu} J_{\mu-l}(k_{II} \xi) k_{II} h_{\mu}^{(2)} + S_l^{cd} \sum_{\mu} J_{\mu-l}(k_{II} \xi) k_{II} h_{\mu}^{(1)} \right], \\ &= \sum_m \sum_{\mu} \left[ \left( \sum_l m \tilde{a}_l^{II} J_{\mu-l}(k_{II} \xi) \right) k_{II} h_{\mu}^{(2)} + \left( \sum_l m \tilde{a}_l^{II} S_l^{cd} J_{\mu-l}(k_{II} \xi) \right) k_{II} h_{\mu}^{(1)} \right]. \end{aligned} \quad (\text{B7})$$

Redefining

$$m \tilde{a}_l^{II} \equiv \sum_{l'} m a_{l'}^{II} J_{l'-l}(k_{II} \xi), \quad (\text{B8})$$

we finally obtain the wave function expressed in unprimed coordinates  $\mathbf{r} = (r, \theta)$  as

$$\begin{aligned} \Psi^{(II)}(\mathbf{r}) &= \sum_m \sum_{l'} m a_{l'}^{II} \times \sum_{\mu} \left[ \left( \sum_l J_{l'-l}(k_{II} \xi) J_{\mu-l}(k_{II} \xi) \right) k_{II} h_{\mu}^{(2)} + \left( \sum_l J_{l'-l}(k_{II} \xi) S_l^{cd} J_{\mu-l}(k_{II} \xi) \right) k_{II} h_{\mu}^{(1)} \right], \\ &= \sum_m \sum_{l'} m a_{l'}^{II} \sum_{\mu} \left[ \delta_{l'\mu} k_{II} h_{\mu}^{(2)} + S_{l'\mu}^{od} k_{II} h_{\mu}^{(1)} \right] = \sum_m \sum_{l'} m a_{l'}^{II} \left[ k_{II} h_{l'}^{(2)} + \sum_{\mu} S_{l'\mu}^{od} k_{II} h_{\mu}^{(1)} \right], \end{aligned} \quad (\text{B9})$$

where  ${}^m a_l^{\text{II}}$  are interpreted as the expansion coefficients in the unprimed coordinates. The resulting matrix  $S^{od} \equiv [S_{l'\mu}^{od}]$  characterizes the scattering from the off-centered small inner disk expressed in the unprimed coordinates and is nondiagonal,

$$S^{od} = U^{-1} S^{cd} U, \quad (\text{B10})$$

with the transformation matrices  $U = [U_{l\mu}] = [J_{\mu-l}(k_{\text{II}}\xi)]$ ,  $U^{-1} = [U_{l'\mu}^{-1}] = [J_{l'-l}(k_{\text{II}}\xi)]$  is responsible for the eccentric displacement/deformation and  $S^{cd} = [S_l^{cd} \delta_{ll'}]$  is the diagonal scattering matrix for the centered inner disk scatterer in the primed coordinates with elements  $S_l^{cd}$  given by Eqs. (B4) and (B5).

The  $S$ -matrix of the whole scatterer can thus be determined by the matching conditions at the outer boundary  $|\mathbf{r}| = R_1$ . In particular, for a given incident spin-1 wave with angular momentum  $m$ , wave-function matching imposing on each momentum state  $j$  yields

$$s_{\text{I}} H_m^{(2)}(k_{\text{I}} R_1) \delta_{mj} + s_{\text{I}} S_{mj} H_j^{(1)}(k_{\text{I}} R_1) = s_{\text{II}} {}^m a_j^{\text{II}} H_m^{(2)}(k_{\text{II}} R_1) + s_{\text{II}} \sum_l {}^m a_l^{\text{II}} S_{lj}^{od} H_j^{(1)}(k_{\text{II}} R_1), \quad (\text{B11a})$$

$$\begin{aligned} & [H_{m-1}^{(2)}(k_{\text{I}} R_1) \delta_{mj} + S_{mj} H_{j-1}^{(1)}(k_{\text{I}} R_1)] - [H_{m+1}^{(2)}(k_{\text{I}} R_1) \delta_{mj} + S_{mj} H_{j+1}^{(1)}(k_{\text{I}} R_1)] \\ &= \left[ {}^m a_j^{\text{II}} H_{j-1}^{(2)}(k_{\text{II}} R_1) + \sum_l {}^m a_l^{\text{II}} S_{lj}^{od} H_{j-1}^{(1)}(k_{\text{II}} R_1) \right] - \left[ {}^m a_j^{\text{II}} H_{j+1}^{(2)}(k_{\text{II}} R_1) + \sum_l {}^m a_l^{\text{II}} S_{lj}^{od} H_{j+1}^{(1)}(k_{\text{II}} R_1) \right]. \end{aligned} \quad (\text{B11b})$$

Defining matrices

$$\begin{cases} \mathbb{X}^{(1,2)} = [H_m^{(1,2)}(k_0 R_1) \delta_{mj}], \\ \mathbb{Y}^{(1,2)} = [H_{m+1}^{(1,2)}(k_0 R_1) \delta_{mj}], \\ \mathbb{Z}^{(1,2)} = [H_{m-1}^{(1,2)}(k_0 R_1) \delta_{mj}], \end{cases} \quad (\text{B12})$$

$$\begin{cases} \mathbf{x}^{(1,2)} = [H_m^{(1,2)}(k_1 R_1) \delta_{mj}], \\ \mathbf{y}^{(1,2)} = [H_{m+1}^{(1,2)}(k_1 R_1) \delta_{mj}], \\ \mathbf{z}^{(1,2)} = [H_{m-1}^{(1,2)}(k_1 R_1) \delta_{mj}], \end{cases} \quad (\text{B13})$$

we can rewrite the equations above in the following compact form:

$$s_{\text{I}} \mathbb{X}^{(2)} + s_{\text{I}} S \mathbb{X}^{(1)} = s_{\text{II}} \mathbb{A} \mathbf{x}^{(2)} + s_{\text{II}} \mathbb{A} S^{od} \mathbf{x}^{(1)}, \quad (\text{B14a})$$

$$\begin{aligned} (\mathbb{Z}^{(2)} - \mathbb{Y}^{(2)}) + S(\mathbb{Z}^{(1)} - \mathbb{Y}^{(1)}) &= \mathbb{A}(\mathbf{z}^{(2)} + S^{od} \mathbf{z}^{(1)}) \\ &\quad - \mathbb{A}(\mathbf{y}^{(2)} + S^{od} \mathbf{y}^{(1)}), \end{aligned} \quad (\text{B14b})$$

with the definition of the coefficient matrix  $\mathbb{A} = [{}^m a_j^{\text{II}}]$ . Solving the equations, we finally arrive at the resulting  $S$  matrix:

$$S = -\frac{\mathbb{Z}^{(2)} - \mathbb{Y}^{(2)} - s_{\text{I}} s_{\text{II}} \mathbb{X}^{(2)} \mathbb{T}}{\mathbb{Z}^{(1)} - \mathbb{Y}^{(1)} - s_{\text{I}} s_{\text{II}} \mathbb{X}^{(1)} \mathbb{T}}, \quad (\text{B15})$$

and

$$\mathbb{A} = \frac{s_{\text{I}}}{s_{\text{II}}} [\mathbb{X}^{(2)} + S \mathbb{X}^{(1)}] \mathbb{F}^{-1}, \quad (\text{B16})$$

where  $s_{\text{I,II}}$  denote the band indices in the corresponding regions,  $\mathbb{T} = \mathbb{F}^{-1}(\mathbb{H} - \mathbb{G})$  with the conventions  $\mathbb{F} = \mathbf{x}^{(2)} + S^{od} \mathbf{x}^{(1)}$ ,  $\mathbb{G} = \mathbf{y}^{(2)} + S^{od} \mathbf{y}^{(1)}$ ,  $\mathbb{H} = \mathbf{z}^{(2)} + S^{od} \mathbf{z}^{(1)}$ .

Inside the inner disk region, i.e.,  $|\mathbf{r}'| < R_2$ , the wavefunction in the primed polar coordinates  $\mathbf{r}' = (r', \theta')$  (with origin at the small disk center  $O'$ ) is

$$\tilde{\Psi}^{(\text{III})}(r', \theta') = \sum_m \sum_l \frac{{}^m \tilde{b}_l}{2} \begin{pmatrix} J_{l-1}(k_{\text{III}} r') e^{-i\theta'} \\ i\sqrt{2} s_{\text{III}} J_l(k_{\text{III}} r') e^{i\theta'} \\ -J_{l+1}(k_{\text{III}} r') e^{i\theta'} \end{pmatrix}. \quad (\text{B17})$$

The expansion coefficients  ${}^m \tilde{b}_l$  can be determined by the matching condition at the inner boundary  $r' = |\mathbf{r} - \xi| = R_2$  between  $\tilde{\Psi}^{(\text{III})}$  and  $\tilde{\Psi}^{(1)}$  [c.f. Eq. (B3)] as

$${}^m \tilde{b}_l = s_{\text{II}} \sum_{l'} {}^m a_{l'}^{\text{II}} J_{l'-l}(k_{\text{II}} \xi) \frac{H_l^{(2)}(k_{\text{II}} R_2) + S_l^{cd} H_l^{(1)}(k_{\text{II}} R_2)}{s_{\text{III}} J_l(k_{\text{III}} R_2)}. \quad (\text{B18})$$

With these expansion coefficients  ${}^m a_l^{\text{II}}$ ,  ${}^m \tilde{b}_l$  and the scattering matrices  $S$ ,  $S^{od}$ ,  $S^{cd}$  obtained in the related regions via Eqs. (B16) and (B18) and Eqs. (B15), (B10), and (B4), respectively, the resulting wave functions in different regions can be calculated correspondingly. Together, they give the full wave function in the entire space.

- [1] M. C. Gutzwiller, *Chaos in Classical and Quantum Mechanics* (Springer, New York, 1991).
- [2] H.-J. Stöckmann, *Quantum Chaos: An Introduction* (Cambridge University Press, New York, 1999).
- [3] P. Gaspard, Quantum chaotic scattering, *Scholarpedia* **9**, 9806 (2014), revision #143296.

- [4] W. H. Miller, Semiclassical limit of quantum mechanical transition state theory for nonseparable systems, *J. Chem. Phys.* **62**, 1899 (1975).
- [5] R. Blümel and U. Smilansky, Classical Irregular Scattering and its Quantum-Mechanical Implications, *Phys. Rev. Lett.* **60**, 477 (1988).

- [6] R. Blümel and U. Smilansky, A simple-model for chaotic scattering: II. Quantum-mechanical theory, *Physica D* **36**, 111 (1989).
- [7] Y.-C. Lai, R. Blümel, E. Ott, and C. Grebogi, Quantum Manifestations of Chaotic Scattering, *Phys. Rev. Lett.* **68**, 3491 (1992).
- [8] H. Cao and J. Wiersig, Dielectric microcavities: Model systems for wave chaos and non-Hermitian physics, *Rev. Mod. Phys.* **87**, 61 (2015).
- [9] J. U. Nöckel, A. D. Stone, and R. K. Chang,  $Q$  spoiling and directionality in deformed ring cavities, *Opt. Lett.* **19**, 1693 (1994).
- [10] A. Mekis, J. U. Nöckel, G. Chen, A. D. Stone, and R. K. Chang, Ray Chaos and  $Q$  Spoiling in Lasing Droplets, *Phys. Rev. Lett.* **75**, 2682 (1995).
- [11] J. U. Nöckel and A. D. Stone, Ray and wave chaos in asymmetric resonant optical cavities, *Nature* **385**, 45 (1997).
- [12] R. A. Jalabert, H. U. Baranger, and A. D. Stone, Conductance Fluctuations in the Ballistic Regime—A Probe of Quantum Chaos? *Phys. Rev. Lett.* **65**, 2442 (1990).
- [13] C. M. Marcus, A. J. Rimberg, R. M. Westervelt, P. F. Hopkins, and A. C. Gossard, Conductance Fluctuations and Chaotic Scattering in Ballistic Microstructures, *Phys. Rev. Lett.* **69**, 506 (1992).
- [14] R. Ketzmerick, Fractal conductance fluctuations in generic chaotic cavities, *Phys. Rev. B* **54**, 10841 (1996).
- [15] A. S. Sachrajda, R. Ketzmerick, C. Gould, Y. Feng, P. J. Kelly, A. Delage, and Z. Wasilewski, Fractal Conductance Fluctuations in a Soft-Wall Stadium and a Sinai Billiard, *Phys. Rev. Lett.* **80**, 1948 (1998).
- [16] B. Huckestein, R. Ketzmerick, and C. H. Lewenkopf, Quantum Transport Through Ballistic Cavities: Soft vs Hard Quantum Chaos, *Phys. Rev. Lett.* **84**, 5504 (2000).
- [17] A. Bäcker, A. Manze, B. Huckestein, and R. Ketzmerick, Isolated resonances in conductance fluctuations and hierarchical states, *Phys. Rev. E* **66**, 016211 (2002).
- [18] R. Yang, L. Huang, Y.-C. Lai, and L. M. Pecora, Modulating quantum transport by transient chaos, *Appl. Phys. Lett.* **100**, 093105 (2012).
- [19] R. Yang, L. Huang, Y.-C. Lai, C. Grebogi, and L. M. Pecora, Harnessing quantum transport by transient chaos, *Chaos* **23**, 013125 (2013).
- [20] P. Strange, *Relativistic Quantum Mechanics: With Applications in Condensed Matter and Atomic Physics* (Cambridge University Press, Cambridge, UK, 1998).
- [21] M. Katsnelson, K. Novoselov, and A. Geim, Chiral tunneling and the Klein paradox in graphene, *Nat. Phys.* **2**, 620 (2006).
- [22] C. W. J. Beenakker, Colloquium: Andreev reflection and Klein tunneling in graphene, *Rev. Mod. Phys.* **80**, 1337 (2008).
- [23] R. Yang, L. Huang, Y.-C. Lai, and C. Grebogi, Abnormal electron paths induced by Klein tunneling in graphene quantum point contacts, *Phys. Rev. B* **84**, 035426 (2011).
- [24] B. Sutherland, Localization of electronic wave functions due to local topology, *Phys. Rev. B* **34**, 5208 (1986).
- [25] D. Bercioux, D. F. Urban, H. Grabert, and W. Häusler, Massless Dirac-Weyl fermions in a  $T_3$  optical lattice, *Phys. Rev. A* **80**, 063603 (2009).
- [26] R. Shen, L. B. Shao, B. Wang, and D. Y. Xing, Single Dirac cone with a flat band touching on line-centered-square optical lattices, *Phys. Rev. B* **81**, 041410(R) (2010).
- [27] D. Green, L. Santos, and C. Chamon, Isolated flat bands and spin-1 conical bands in two-dimensional lattices, *Phys. Rev. B* **82**, 075104 (2010).
- [28] B. Dóra, J. Kailasvuori, and R. Moessner, Lattice generalization of the Dirac equation to general spin and the role of the flat band, *Phys. Rev. B* **84**, 195422 (2011).
- [29] F. Wang and Y. Ran, Nearly flat band with Chern number  $c = 2$  on the dice lattice, *Phys. Rev. B* **84**, 241103(R) (2011).
- [30] X. Huang, Y. Lai, Z. H. Hang, H. Zheng, and C. T. Chan, Dirac cones induced by accidental degeneracy in photonic crystals and zero-refractive-index materials, *Nat. Mater.* **10**, 582 (2011).
- [31] J. Mei, Y. Wu, C. T. Chan, and Z.-Q. Zhang, First-principles study of Dirac and Dirac-like cones in phononic and photonic crystals, *Phys. Rev. B* **86**, 035141 (2012).
- [32] P. Moitra, Y. Yang, Z. Anderson, I. I. Kravchenko, D. P. Briggs, and J. Valentine, Realization of an all-dielectric zero-index optical metamaterial, *Nat. Photonics* **7**, 791 (2013).
- [33] A. Raoux, M. Morigi, J.-N. Fuchs, F. Piéchon, and G. Montambaux, From Dia- To Paramagnetic Orbital Susceptibility of Massless Fermions, *Phys. Rev. Lett.* **112**, 026402 (2014).
- [34] D. Guzmán-Silva, C. Mejía-Cortés, M. A. Bandres, M. C. Rechtsman, S. Weimann, S. Nolte, M. Segev, A. Szameit, and R. A. Vicencio, Experimental observation of bulk and edge transport in photonic Lieb lattices, *New J. Phys.* **16**, 063061 (2014).
- [35] J. Romhányi, K. Penc, and R. Ganesh, Hall effect of triplons in a dimerized quantum magnet, *Nat. Commun.* **6**, 6805 (2015).
- [36] G. Giovannetti, M. Capone, J. van den Brink, and C. Ortix, Kekulé textures, pseudospin-one Dirac cones, and quadratic band crossings in a graphene-hexagonal indium chalcogenide bilayer, *Phys. Rev. B* **91**, 121417(R) (2015).
- [37] Y. Li, S. Kita, P. Muoz, O. Reshef, D. I. Vulis, M. Yin, M. Lonar, and E. Mazur, On-chip zero-index metamaterials, *Nat. Photonics* **9**, 738 (2015).
- [38] S. Mukherjee, A. Spracklen, D. Choudhury, N. Goldman, P. Öhberg, E. Andersson, and R. R. Thomson, Observation of a Localized Flat-Band State in a Photonic Lieb Lattice, *Phys. Rev. Lett.* **114**, 245504 (2015).
- [39] R. A. Vicencio, C. Cantillano, L. Morales-Inostroza, B. Real, C. Mejía-Cortés, S. Weimann, A. Szameit, and M. I. Molina, Observation of Localized States in Lieb Photonic Lattices, *Phys. Rev. Lett.* **114**, 245503 (2015).
- [40] S. Taie, H. Ozawa, T. Ichinose, T. Nishio, S. Nakajima, and Y. Takahashi, Coherent driving and freezing of bosonic matter wave in an optical Lieb lattice, *Sci. Adv.* **1**, e1500854 (2015).
- [41] A. Fang, Z. Q. Zhang, S. G. Louie, and C. T. Chan, Klein tunneling and supercollimation of pseudospin-1 electromagnetic waves, *Phys. Rev. B* **93**, 035422 (2016).
- [42] F. Diebel, D. Leykam, S. Kroesen, C. Denz, and A. S. Desyatnikov, Conical Diffraction and Composite Lieb Bosons in Photonic Lattices, *Phys. Rev. Lett.* **116**, 183902 (2016).
- [43] L. Zhu, S.-S. Wang, S. Guan, Y. Liu, T. Zhang, G. Chen, and S. A. Yang, Blue phosphorene oxide: Strain-tunable quantum phase transitions and novel 2d emergent fermions, *Nano Lett.* **16**, 6548 (2016).
- [44] B. Bradlyn, J. Cano, Z. Wang, M. G. Vergniory, C. Felser, R. J. Cava, and B. A. Bernevig, Beyond Dirac and Weyl fermions: Unconventional quasiparticles in conventional crystals, *Science* **353** (2016).

- [45] I. C. Fulga and A. Stern, Triple point fermions in a minimal symmorphic model, *Phys. Rev. B* **95**, 241116(R) (2017).
- [46] M. Ezawa, Triplet fermions and Dirac fermions in borophene, *Phys. Rev. B* **96**, 035425 (2017).
- [47] C. Zhong, Y. Chen, Z.-M. Yu, Y. Xie, H. Wang, S. A. Yang, and S. Zhang, Three-dimensional pentagon carbon with a genesis of emergent fermions, *Nat. Commun.* **8**, 15641 (2017).
- [48] Y.-Q. Zhu, D.-W. Zhang, H. Yan, D.-Y. Xing, and S.-L. Zhu, Emergent pseudospin-1 maxwell fermions with a three-fold degeneracy in optical lattices, *Phys. Rev. A* **96**, 033634 (2017).
- [49] R. Drost, T. Ojanen, A. Harju, and P. Liljeroth, Topological states in engineered atomic lattices, *Nat. Phys.* **13**, 668 (2017).
- [50] M. R. Slot, T. S. Gardenier, P. H. Jacobse, G. C. P. van Miert, S. N. Kempkes, S. J. M. Zevenhuizen, C. M. Smith, D. Vanmaekelbergh, and I. Swart, Experimental realization and characterization of an electronic Lieb lattice, *Nat. Phys.* **13**, 672 (2017).
- [51] X. Tan, D.-W. Zhang, Q. Liu, G. Xue, H.-F. Yu, Y.-Q. Zhu, H. Yan, S.-L. Zhu, and Y. Yu, Topological Maxwell Metal Bands in a Superconducting Qutrit, *Phys. Rev. Lett.* **120**, 130503 (2018).
- [52] S. Kocaman, M. S. Aras, P. Hsieh, J. F. McMillan, C. G. Biris, N. C. Panoiu, M. B. Yu, D. L. Kwong, A. Stein, and C. W. Wong, Zero phase delay in negative-index photonic crystal superlattices, *Nat. Photonics* **5**, 499 (2011).
- [53] P. Hsieh, C. Chung, J. F. McMillan, M. Tsai, M. Lu, N. C. Panoiu, and C. W. Wong, Photon transport enhanced by transverse anderson localization in disordered superlattices, *Nat. Phys.* **11**, 268 (2015).
- [54] D. F. Urban, D. Bercioux, M. Wimmer, and W. Häusler, Barrier transmission of Dirac-like pseudospin-one particles, *Phys. Rev. B* **84**, 115136 (2011).
- [55] V. V. Cheianov, V. Fal'ko, and B. L. Altshuler, The focusing of electron flow and a Veselago lens in graphene  $p$ - $n$  junctions, *Science* **315**, 1252 (2007).
- [56] G.-H. Lee, G.-H. Park, and H.-J. Lee, Observation of negative refraction of Dirac fermions in graphene, *Nat. Phys.* **11**, 925 (2015).
- [57] S. Chen, Z. Han, M. M. Elahi, K. M. M. Habib, L. Wang, B. Wen, Y. Gao, T. Taniguchi, K. Watanabe, J. Hone, A. W. Ghosh, and C. R. Dean, Electron optics with  $p$ - $n$  junctions in ballistic graphene, *Science* **353**, 1522 (2016).
- [58] R. Akis, D. K. Ferry, and J. P. Bird, Wave Function Scarring Effects in Open Stadium Shaped Quantum Dots, *Phys. Rev. Lett.* **79**, 123 (1997).
- [59] R. Akis, J. P. Bird, and D. K. Ferry, The persistence of eigenstates in open quantum dots, *Appl. Phys. Lett.* **81**, 129 (2002).
- [60] T. Harayama, P. Davis, and K. S. Ikeda, Stable Oscillations of a Spatially Chaotic Wave Function in a Microstadium Laser, *Phys. Rev. Lett.* **90**, 063901 (2003).
- [61] S.-Y. Lee, M. S. Kurdoglyan, S. Rim, and C.-M. Kim, Resonance patterns in a stadium-shaped microcavity, *Phys. Rev. A* **70**, 023809 (2004).
- [62] W. Fang, A. Yamilov, and H. Cao, Analysis of high-quality modes in open chaotic microcavities, *Phys. Rev. A* **72**, 023815 (2005).
- [63] M. Leubental, J. S. Lauret, R. Hierle, and J. Zyss, Highly directional stadium-shaped polymer microlasers, *Appl. Phys. Lett.* **88**, 031108 (2006).
- [64] R. Yang, L. Huang, Y.-C. Lai, and C. Grebogi, Quantum chaotic scattering in graphene systems, *Europhys. Lett.* **94**, 40004 (2011).
- [65] J. Cserti, A. Pályi, and C. Péterfalvi, Caustics Due to a Negative Refractive Index in Circular Graphene  $p$ - $n$  Junctions, *Phys. Rev. Lett.* **99**, 246801 (2007).
- [66] J. H. Bardarson, M. Titov, and P. W. Brouwer, Electrostatic Confinement of Electrons in an Integrable Graphene Quantum Dot, *Phys. Rev. Lett.* **102**, 226803 (2009).
- [67] M. Schneider and P. W. Brouwer, Resonant scattering in graphene with a gate-defined chaotic quantum dot, *Phys. Rev. B* **84**, 115440 (2011).
- [68] R. L. Heinisch, F. X. Bronold, and H. Fehske, Mie scattering analog in graphene: Lensing, particle confinement, and depletion of Klein tunneling, *Phys. Rev. B* **87**, 155409 (2013).
- [69] J.-S. Wu and M. M. Fogler, Scattering of two-dimensional massless Dirac electrons by a circular potential barrier, *Phys. Rev. B* **90**, 235402 (2014).
- [70] J. Caridad, S. Connaughton, C. Ott, H. B. Weber, and V. Krstic, An electrical analogy to Mie scattering, *Nat. Commun.* **7**, 12894 (2016).
- [71] C. Gutierrez, L. Brown, C.-J. Kim, J. Park, and A. N. Pasupathy, Klein tunneling and electron trapping in nanometre-scale graphene quantum dots, *Nat. Phys.* **12**, 1069 (2016).
- [72] Y.-C. Lai, L. Huang, H.-Y. Xu, and C. Grebogi, Relativistic quantum chaos—an emergent interdisciplinary field, *Chaos* **28**, 052101 (2018).
- [73] L. Huang, H.-Y. Xu, C. Grebogi, and Y.-C. Lai, Relativistic quantum chaos, *Phys. Rep.* **753**, 1 (2018).
- [74] T. Graß, B. Juliá-Díaz, M. Kuś, and M. Lewenstein, Quantum Chaos in SU(3) Models with Trapped Ions, *Phys. Rev. Lett.* **111**, 090404 (2013).
- [75] H.-Y. Xu and Y.-C. Lai, Revival resonant scattering, perfect caustics, and isotropic transport of pseudospin-1 particles, *Phys. Rev. B* **94**, 165405 (2016).
- [76] J. Wiersig, Boundary element method for resonances in dielectric microcavities, *J. Opt. A: Pure Appl. Opt.* **5**, 53 (2003).
- [77] A. D. Kovács, G. Dávid, B. Dóra, and J. Cserti, Frequency-dependent magneto-optical conductivity in the generalized  $\alpha - T_3$  model, *Phys. Rev. B* **95**, 035414 (2017).
- [78] Y. Leviatan and A. Boag, Analysis of electromagnetic scattering from dielectric cylinders using a multifilament current model, *IEEE Trans. Antennas Propag.* **35**, 1119 (1987).
- [79] M. G. Imhof, Multiple multipole expansions for elastic scattering, *J. Acoust. Soc. Am.* **100**, 2969 (1996).
- [80] D. I. Kaklamani and H. T. Anastassiou, Aspects of the method of auxiliary sources (MAS) in computational electromagnetics, *IEEE Anten. Propag. Mag.* **44**, 48 (2002).
- [81] E. Moreno, D. Erni, C. Hafner, and R. Vahldieck, Multiple multipole method with automatic multipole setting applied to the simulation of surface plasmons in metallic nanostructures, *J. Opt. Soc. Am. A* **19**, 101 (2002).
- [82] G. Tayeb and S. Enoch, Combined fictitious-sources-scattering-matrix method, *J. Opt. Soc. Am. A* **21**, 1417 (2004).
- [83] H.-Y. Xu, G.-L. Wang, L. Huang, and Y.-C. Lai, Chaos in Dirac Electron Optics: Emergence of a Relativistic Quantum Chimera, *Phys. Rev. Lett.* **120**, 124101 (2018).
- [84] E.-A. Y. You, W. Zhou, J. Y. Suh, M. D. Huntington, and T. Odom, Polarization-dependent multipolar plasmon resonances

- in anisotropic multiscale au particles, *ACS Nano* **6**, 1786 (2012).
- [85] E. Doron and U. Smilansky, Semiclassical quantization of chaotic billiards: A scattering theory approach, *Nonlinearity* **5**, 1055 (1992).
- [86] E. Doron and S. D. Frischat, Semiclassical Description of Tunneling in Mixed Systems: Case of the Annular Billiard, *Phys. Rev. Lett.* **75**, 3661 (1995).
- [87] G. Hackenbroich and J. U. Nöckel, Dynamical tunneling in optical cavities, *Europhys. Lett.* **39**, 371 (1997).
- [88] A. I. Rahachou and I. V. Zozoulenko, Effects of boundary roughness on a  $Q$  factor of whispering-gallery-mode lasing microdisk cavities, *J. Appl. Phys.* **94**, 7929 (2003).
- [89] K. Y. Bliokh, D. Smirnova, and F. Nori, Quantum spin Hall effect of light, *Science* **348**, 1448 (2015).
- [90] S. Datta, *Electronic Transport in Mesoscopic Systems* (Cambridge University Press, Cambridge, UK, 1995).
- [91] S. Habib, K. Jacobs, and K. Shizume, Emergence of Chaos in Quantum Systems Far from the Classical Limit, *Phys. Rev. Lett.* **96**, 010403 (2006).
- [92] A. Kapulkin and A. K. Pattanayak, Nonmonotonicity in the Quantum-Classical Transition: Chaos Induced by Quantum Effects, *Phys. Rev. Lett.* **101**, 074101 (2008).
- [93] P. Pechukas, Time-dependent semiclassical scattering theory. II. Atomic collisions, *Phys. Rev.* **181**, 174 (1969).
- [94] H. Frisk and T. Guhr, Spin-orbit coupling in semiclassical approximation, *Ann. Phys.* **221**, 229 (1993).